

# Supporting Information

**Pure Red- Light Emitting Europium based complexes as efficient UV light converters: Synthesis, crystal structure and Photoluminescence properties**

**Asgar Ali,\* Zubair Ahmed, Rahisuddin and K. Iftikhar**

Lanthanide Research Laboratory, Department of Chemistry, Jamia Millia Islamia, New Delhi 110025, India. E-mail corresponding:[asgar.chemistry@gmail.com](mailto:asgar.chemistry@gmail.com)

## Experimental and theoretical Intensity Parameters

Under parity law, electronic transitions within 4f subshells are strictly prohibited. However, electric dipole transition can be observed by mixing of upper shell wave functions into 4f wavefunction due to crystal field effect. These transitions are used in laser sources as they are sharp and narrow band widths. The intensity of the magnetic-dipole transition can be calculated from free ion wave function. However, for induced electric-dipole transitions, dipole strength calculation is difficult, and parameterization is requisite, as provided by the Judd-Ofelt theory<sup>1,2</sup>. In the case of Eu, the intensity of emission transitions can be used to determine the Judd-Ofelt intensity parameters ( $\Omega_\lambda$ ,  $\lambda = 2, 4$ , and  $6$ ). Since the absolute intensities could not be measured, therefore the intensity of the  $^5D_0 \rightarrow ^7F_1$  magnetic-dipole transition is considered as a reference with dipole strength (Dmd) of  $9.6 \times 10^{-42}$  esu<sup>2</sup> cm<sup>2</sup> and the parameters of other transitions are calculated relative to it<sup>3</sup>. The  $\Omega_\lambda$  parameters are calculated using eq S1

$$\Omega_\lambda = \frac{D_m V_1^3}{e^2 V_\lambda^3} \frac{9\eta^3}{[\langle \psi J | U^\lambda | \psi J' \rangle]^2 \eta(\eta^2 + 2)^2} \frac{\int I_\lambda v dv}{\int I_\nu dv}$$

(S1)

where  $v_1$  and  $v_\lambda$  denotes the average wave numbers of  $^5D_0 \rightarrow ^7F_1$  and  $^5D_0 \rightarrow ^7F_\lambda$  transitions

respectively,  $e$  is the electronic charge,  $\frac{\int I_\lambda v dv}{\int I_\nu dv}$  is the ratio of integrated intensity of  $^5D_0 \rightarrow$

$^7F_\lambda$  to the  $^5D_0 \rightarrow ^7F_1$  transition, and  $\eta(\eta^2 + 2)^2$  is the Lorentz local field correction and  $\eta$  is the refractive index of the medium. From literature  $[\langle \psi J | U^\lambda | \psi J' \rangle]^2$  (Square reduced matrix elements) values were obtained<sup>4,5</sup>. There is a proportionality between covalence in bonding and the  $\Omega_2$  parameter, and the higher the value, the more covalency in the bonding. The value of the  $\Omega_2$  parameter is directly proportional to the hypersensitivity of  $^5D_0 \rightarrow ^7F_2$  transition<sup>6</sup>. The  $\Omega_4$

parameter describes the rigidity of the medium in which the Ln (III) ions are located<sup>7</sup>. Since the  $^5D_0 \rightarrow ^7F_6$  transition cannot be measured, the  $\Omega_6$  experimental parameter could not be determined and is thus ignored in calculations.

Using Judd-Ofelt parameters various photophysical quantities like radiative transition probability (A), emission quantum efficiency ( $Q_{Eu}^{Eu}$ ) and radiative lifetime ( $\tau_{rad}$ ) for the transition of Eu<sup>3+</sup> in various phases were calculated. Equation (S2) gives the radiative transition probability (A) between two manifolds  $j$  and  $j'$ .

$$A(\psi_j, \psi_{j'}) = \frac{64\pi^4 v^3}{3h(2j+1)} [\chi D_{ed} + \eta^3 D_{md}] \quad (S2)$$

Where  $D_{ed}$  is dipole strength of electric dipole,  $D_{md}$  is dipole strength of magnetic dipole,  $v$  denotes the transition's average wave number.  $\chi$  is correction factor and  $\eta$  is refractive index. The transition probability (A) for a transition from  $^5D_0$  with  $j$  equal to zero to  $^7F_\lambda$  with  $j$  equaling  $\lambda=0,1,2,3,4,5$  and 6 is calculated from the emission spectra using equation (S3).

$$A_{0-\lambda} = A_{0-1} \frac{S_{0-\lambda} \sigma_\lambda}{S_{0-1} \sigma_1} \quad (S3)$$

where  $S_{0-\lambda}$  and  $\sigma_\lambda$  are area under the  $0 \rightarrow \lambda$  transition of emission spectra and its energy barycentre respectively.  $A_{0-1}$  is the Einstein's coefficient for the  $0 \rightarrow 1$  magnetic-dipole transition and its reported value is  $50\text{s}^{-1}$ . The correlation between lifetime and the transition probabilities (radiative or non-radiative) is given by the equation (S4),

$$A_{tot} = \frac{1}{\tau} = A_{rad} + A_{nrad} \quad (S4)$$

where  $A_{rad}$  is the sum of all radiative probabilities associated with transitions between  $^5D_0 \rightarrow ^7F_\lambda$  with  $\lambda = j$  (equation S5),

$$A_{rad} = \sum_{\lambda=j} A_{0-j} \quad (S5)$$

The inverse of  $A_{rad}$  yields the radiative lifetime  $\tau_{rad}$  of  $^5D_0$  level and the intrinsic quantum yield

$Q_{Eu}^{Eu}$  is given by equation (S6),

$$Q_{Eu}^{Eu} = \frac{A_{rad}}{A_{rad} + A_{nrad}} \quad (S6)$$

The experimental ( $\Omega_\lambda$ ) parameters ( $\lambda = 2, 4$  and  $6$ ) are calculated using the emission spectra and lifetime of the europium ion within the Judd-Ofelt theory. Theoretically the ( $\Omega_\lambda$ ) parameters for Sparkle/PM7 are calculated using equations (S7) and (S8).

$$\Omega_\lambda = (2\lambda + 1) \sum_t^{\lambda - 1, \lambda + 1} \sum_{p=0}^{(odd)t(all)} \frac{|B_{\lambda tp}|^2}{(2t + 1)} \quad (S7)$$

Where the parameter  $B_{\lambda tp} = B_{\lambda tp}^{ed} + B_{\lambda tp}^{dc}$  and is expressed as

$$B_{\lambda tp} = \frac{2}{\Delta E} \langle r^{t+1} \rangle \theta(t, \lambda) \gamma_p^t \left[ \frac{(\lambda + 1)(2\lambda + 3)}{2\lambda + 1} \right]^{\frac{1}{2}} \times \langle r^\lambda \rangle (1 - \sigma_\lambda) \langle f \| C^{(\lambda)} \| f \rangle \Gamma_p^t \delta_{t, \lambda + 1} \quad (S8)$$

The theoretical  $\Omega_\lambda$  parameters are derived by adjusting the charge factor ( $g$ ) and polarizabilities ( $\alpha$ ) appearing in equation S9 and S10, respectively, to reproduce the phenomenological (experimental) values for  $\Omega_2$  and  $\Omega_4$ .

$$\gamma_p^t = \left( \frac{4\pi}{2t + 1} \right)^{\frac{1}{2}} e^2 \sum_j \rho_j (2\beta_j)^{t+1} \frac{g_j}{R_j^{t+1}} Y_p^t (\theta_j, \varphi_j) \quad (S9)$$

$$\Gamma_p^t = \left( \frac{4\pi}{2t + 1} \right)^{\frac{1}{2}} \sum_j \frac{\alpha_j}{R_j^{t+1}} Y_p^t (\theta_j, \varphi_j) \quad (S10)$$

In equation S9,  $\gamma_p^t$  ( $t = 1, 3, 5$  and  $7$ ) contain the sum over of the odd-rank ligand field parameters<sup>42</sup> of the surrounding atoms. Similarly, in equation S10,  $T_p^t$  ( $t = 1, 3, 5$  and  $7$ ) parameter contains the effect of the chemical environment on the overall coordination geometry

around the lanthanide ion. The data obtained from these equations are tabulated in Table 5.

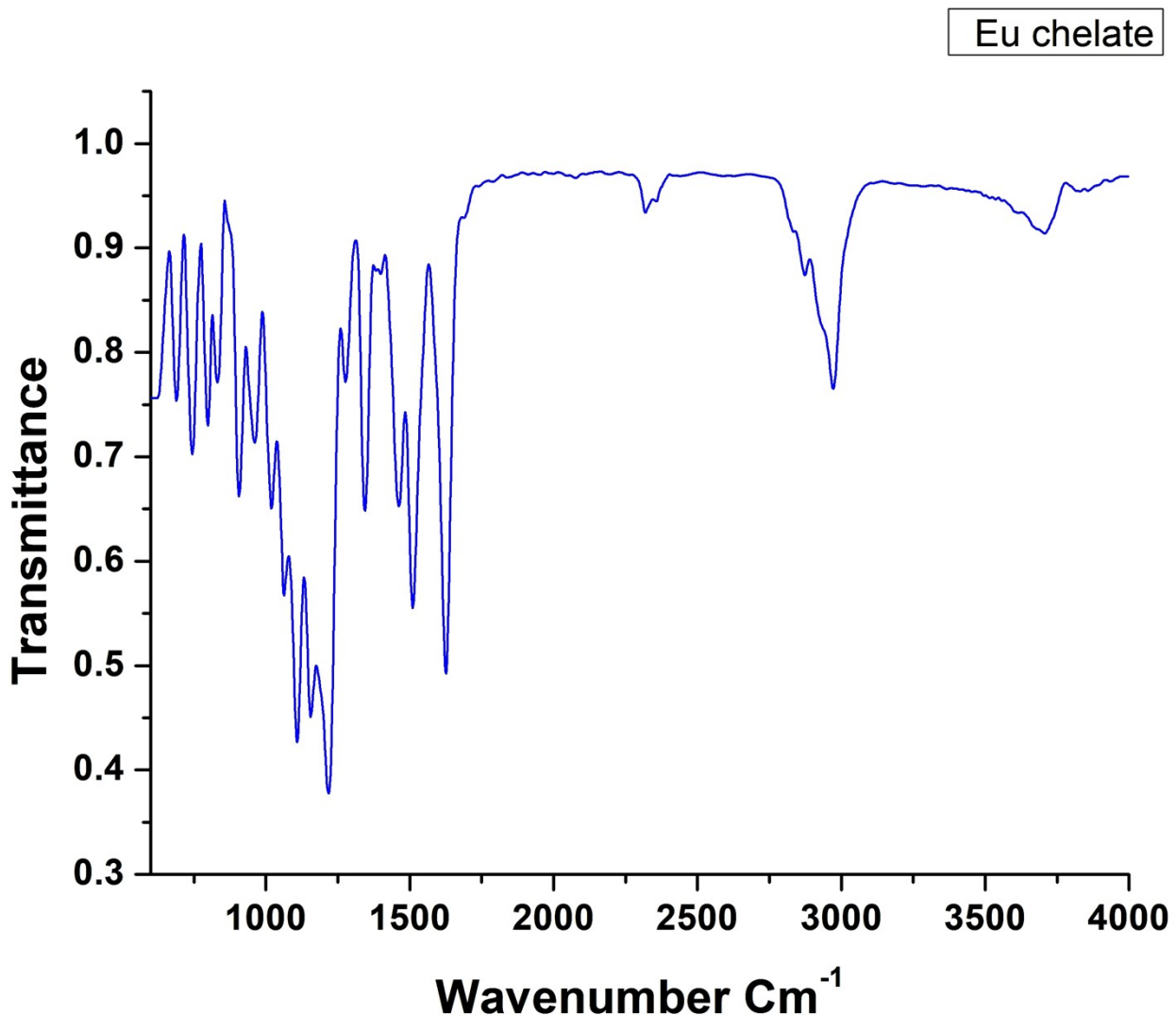


**Fig. S1.** IR spectra of the Europium chelate.

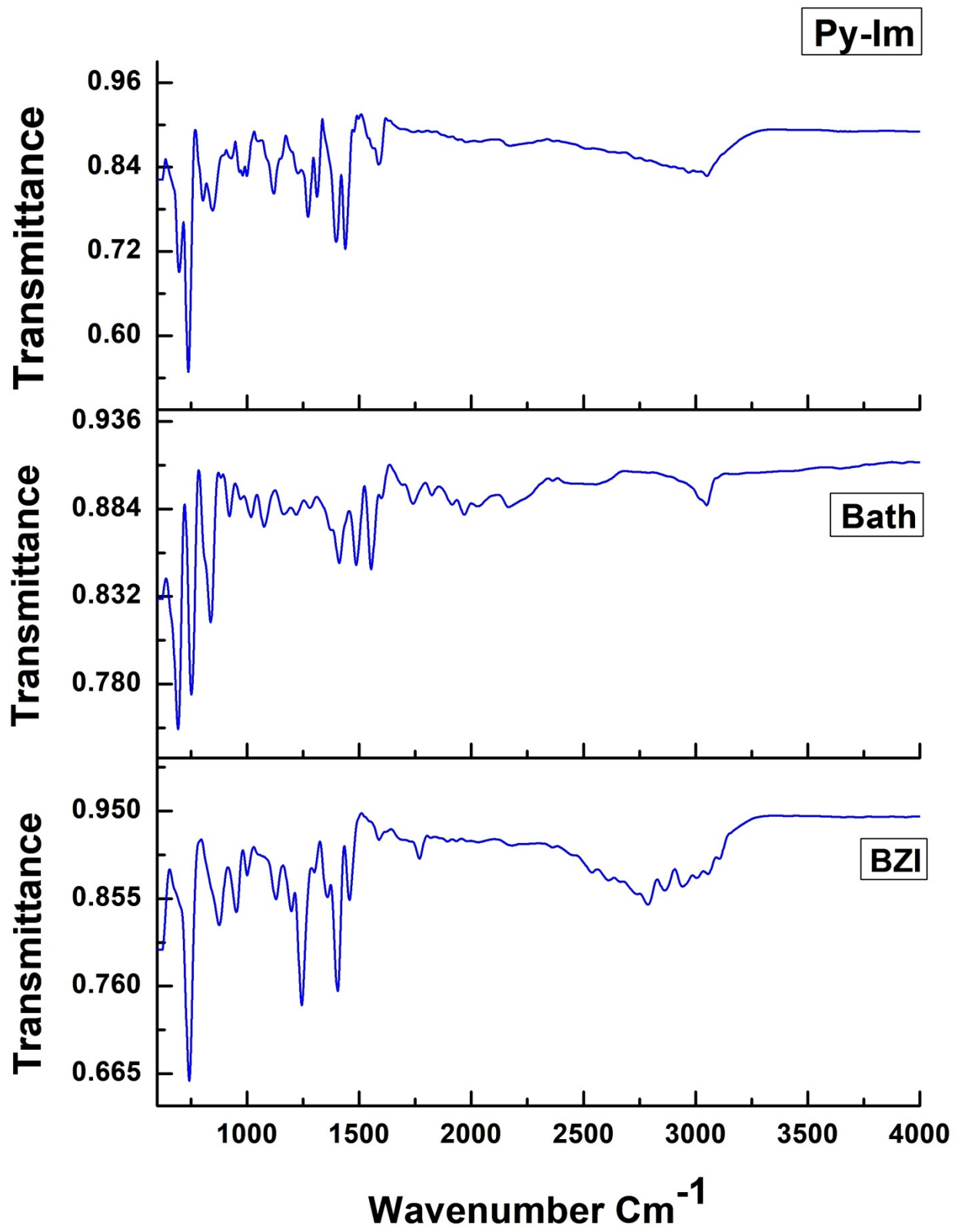


**Fig. S2.** IR spectra of ligands.

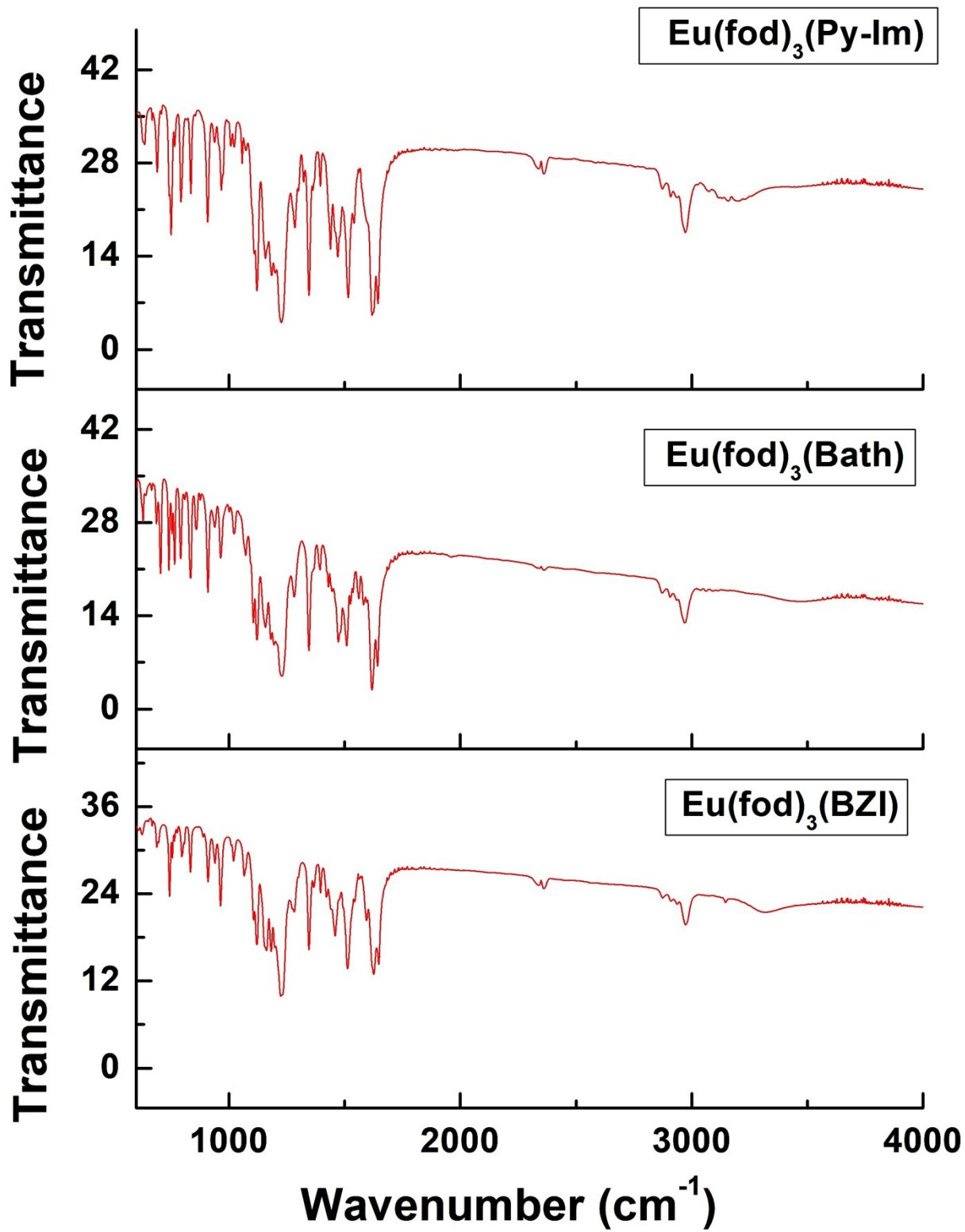
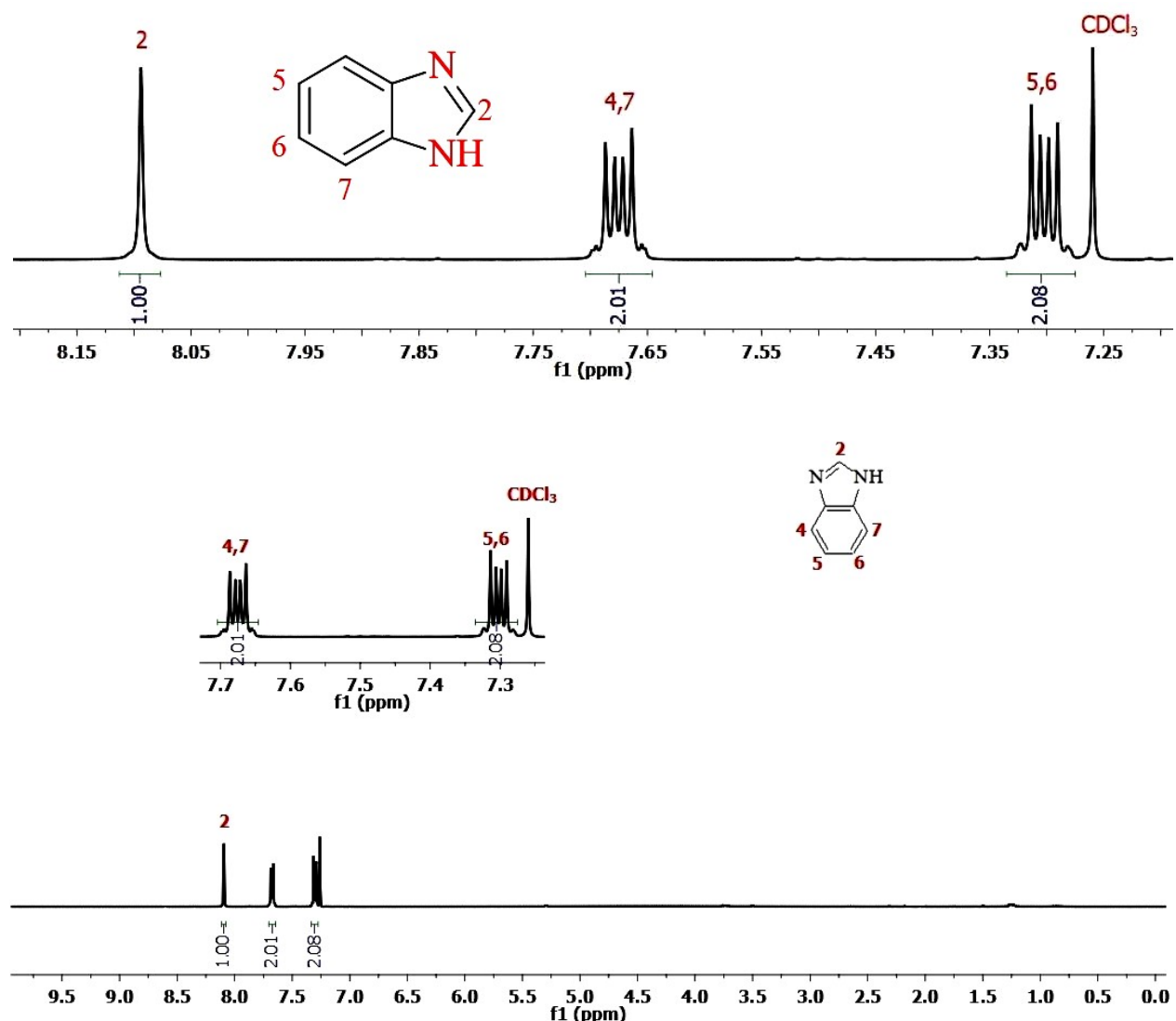
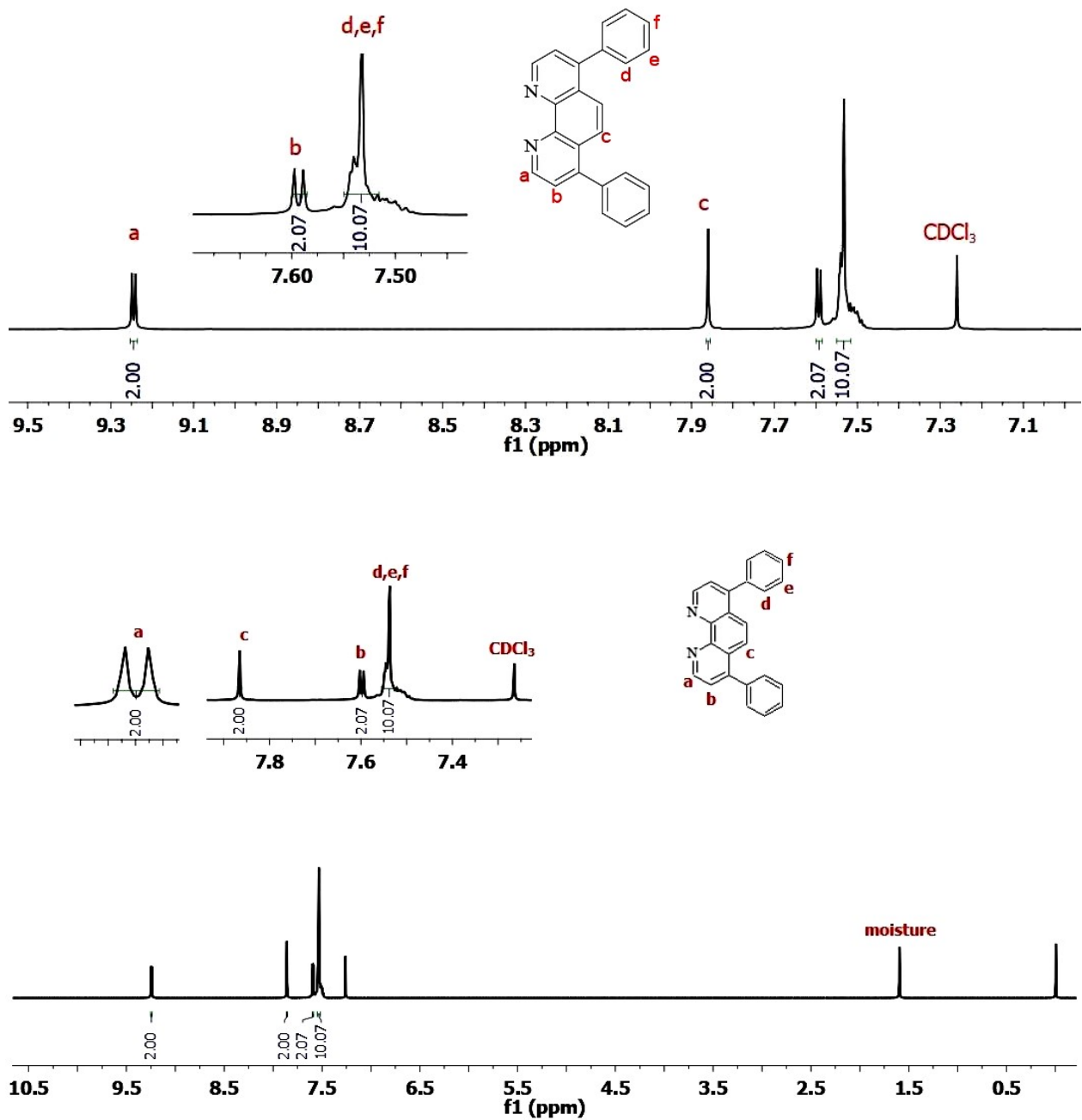


Fig. S3. IR Spectra of the complexes.



**Fig. S4.** 500 MHz  $^1\text{H}$  NMR spectra at 298 K of Benzimidazole (bzi) in  $\text{CDCl}_3$ .



**Fig. S5.** 500 MHz  $^1\text{H}$  NMR spectra at 298 K of bathophenanthroline (bath) in  $\text{CDCl}_3$ .

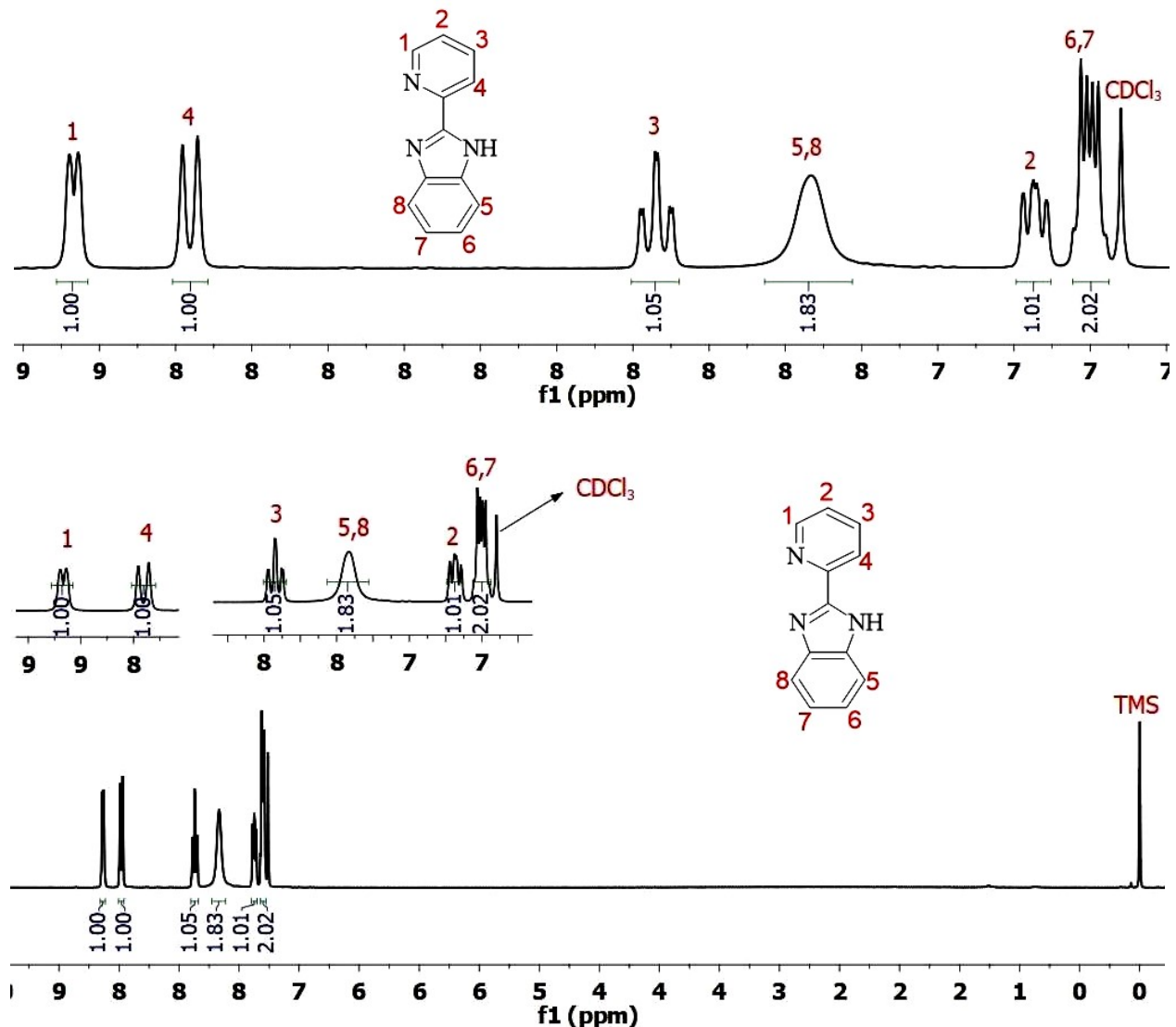


**Fig. S6.** 500 MHz  $^1\text{H}$  NMR spectra at 298 K of 2-(2-pyridyl)benzimidazole (py-im) in  $\text{CDCl}_3$ .

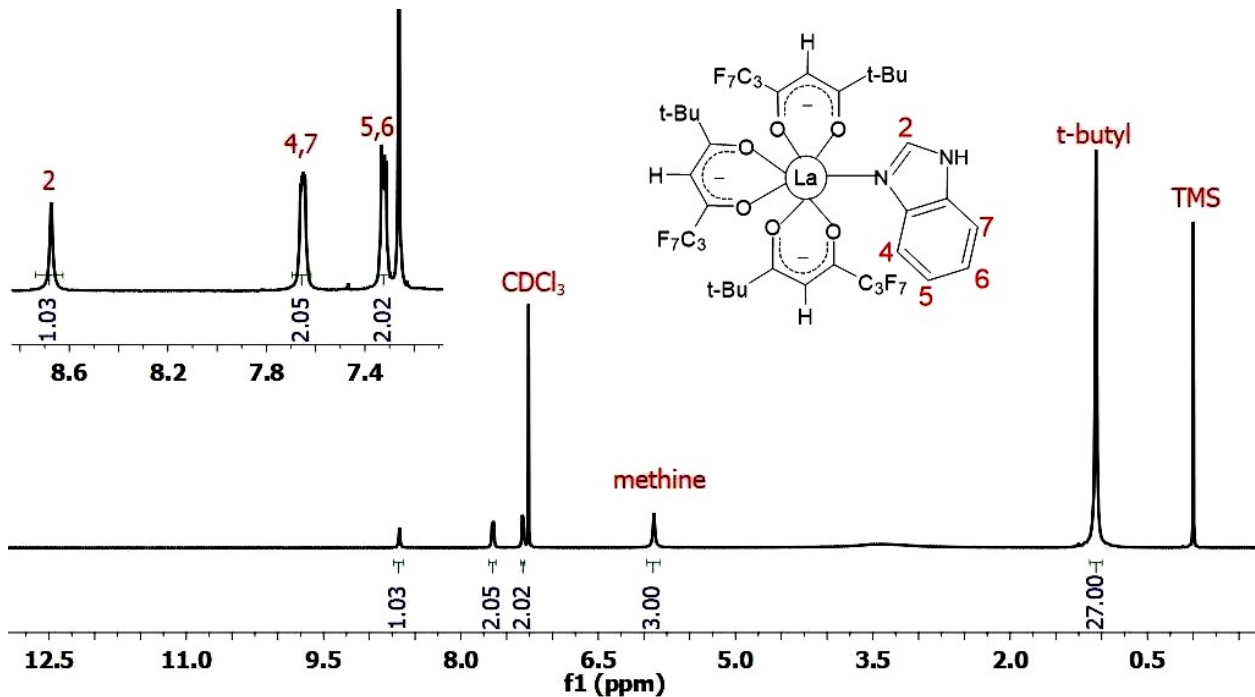


**Fig. S7.** 500 MHz <sup>1</sup>H NMR spectra at 298 K of La(fod)<sub>3</sub>(bzi) in CDCl<sub>3</sub>.

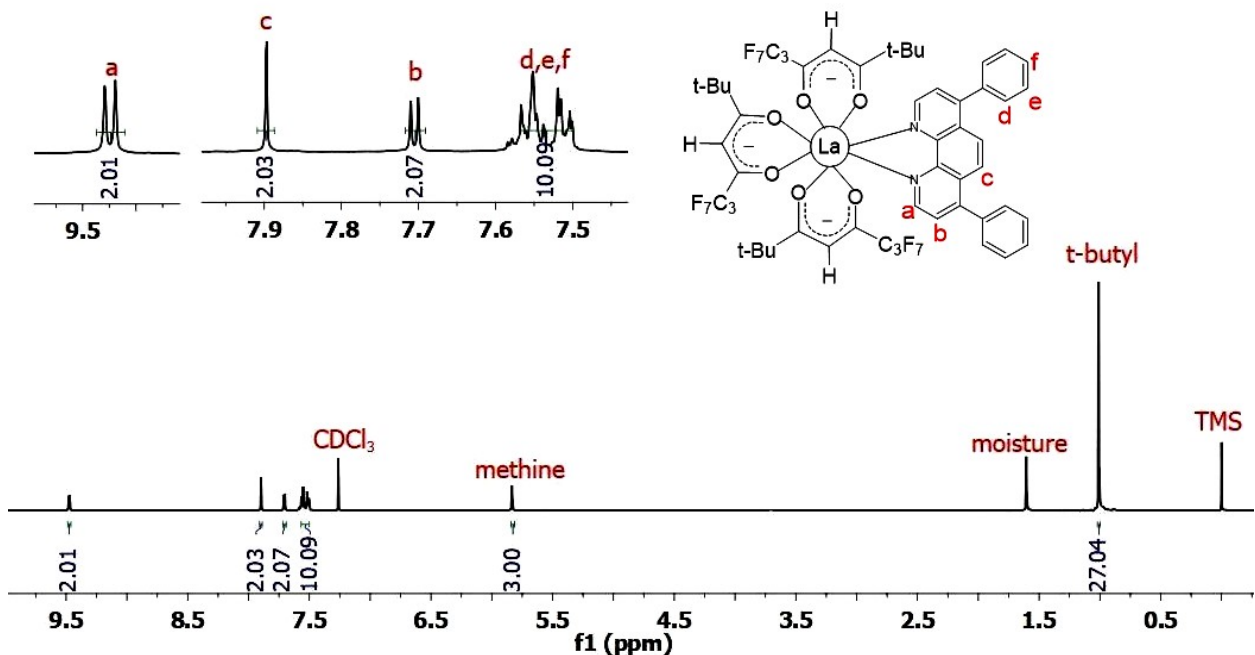


**Fig. S8.** 500 MHz <sup>1</sup>H NMR spectra at 298 K of [La(fod)<sub>3</sub>(bath)] in CDCl<sub>3</sub>.

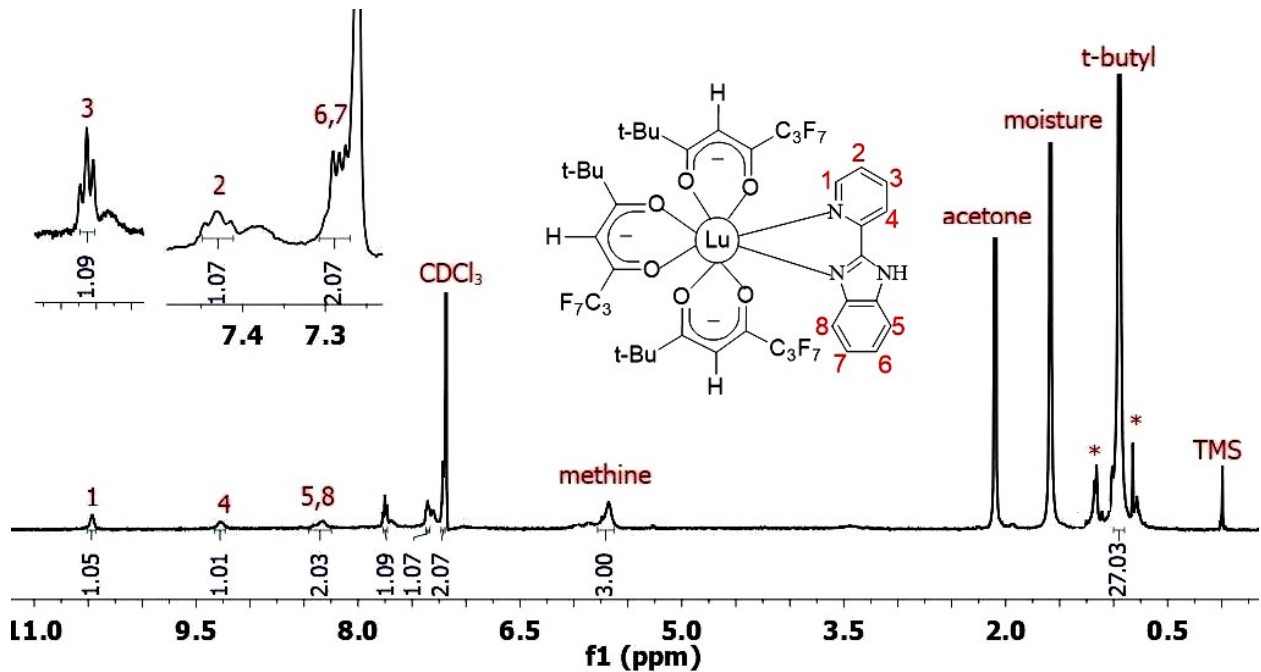
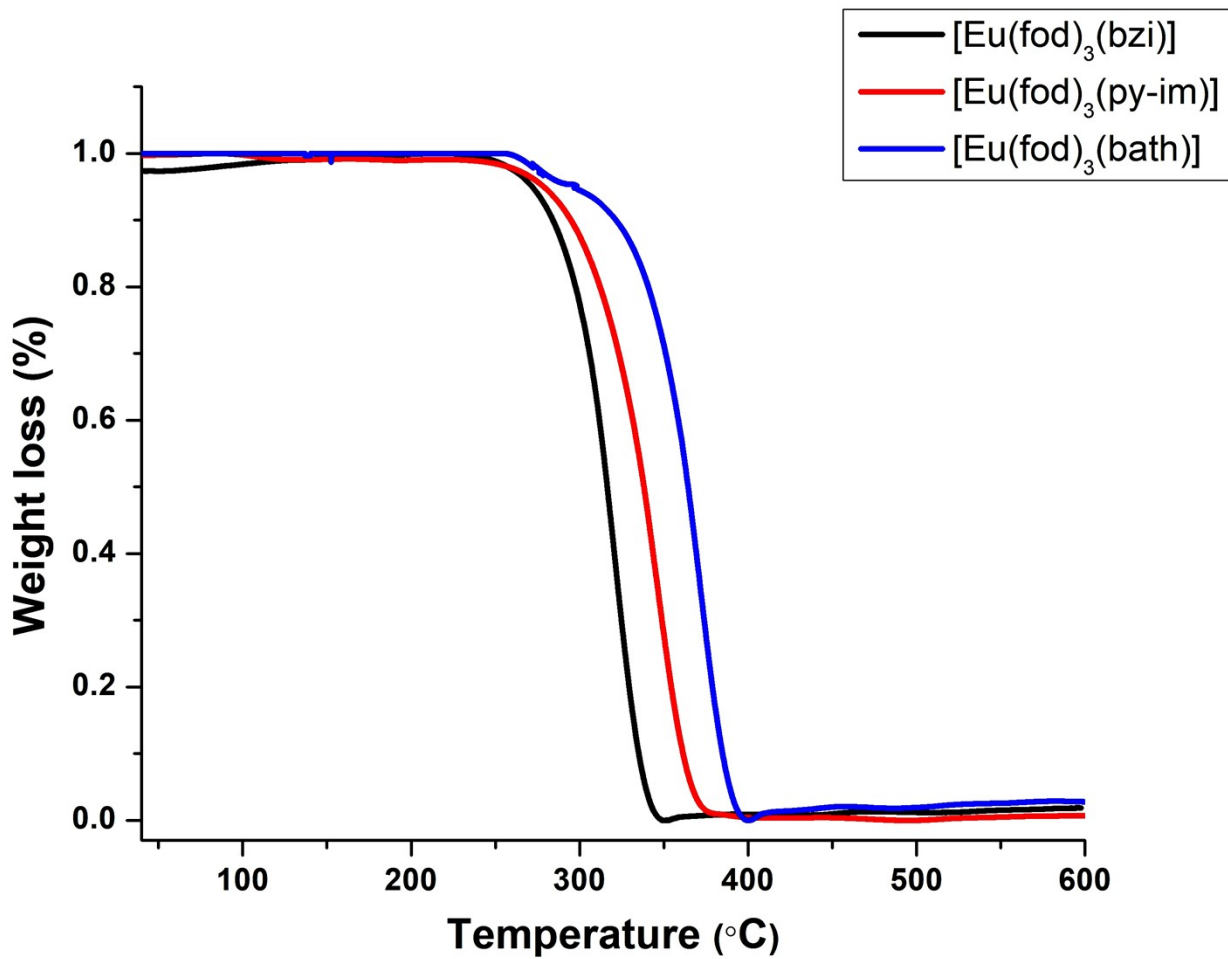
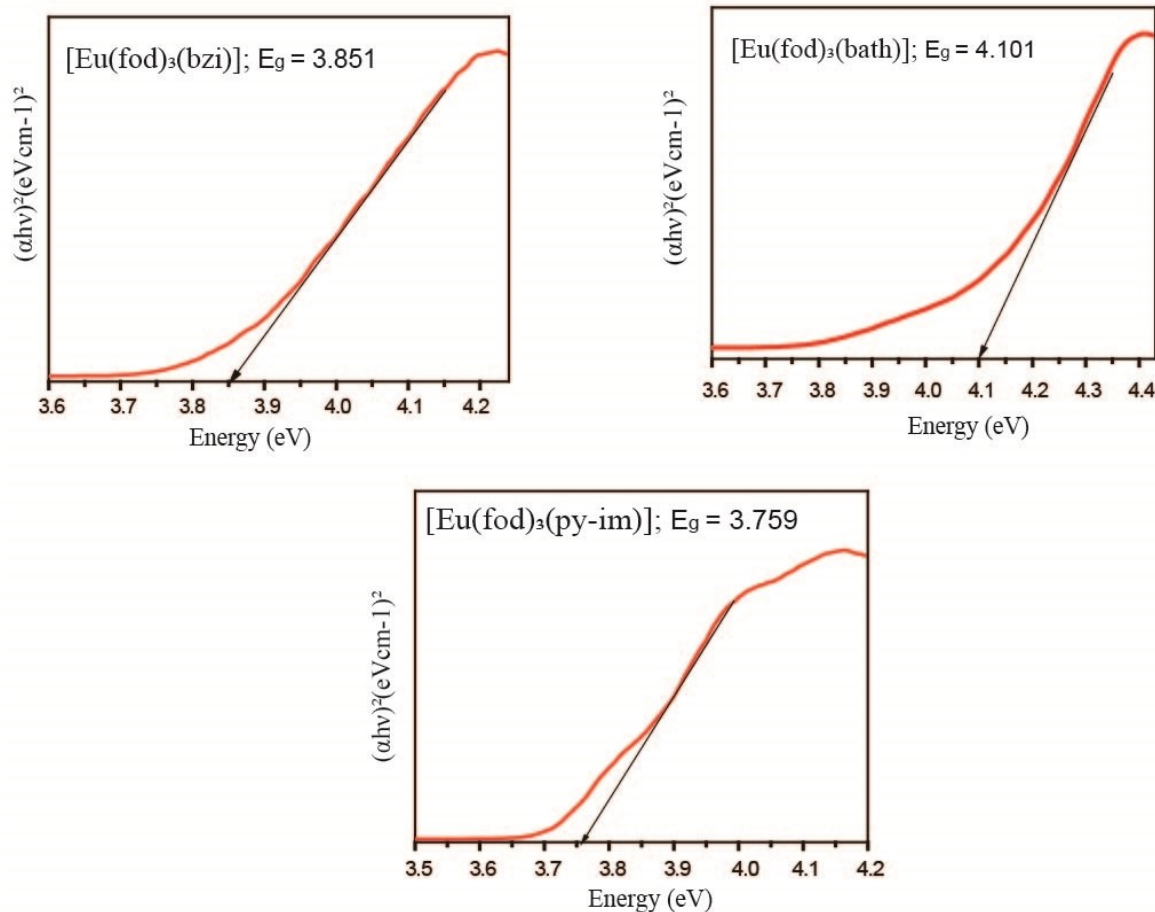


Fig. S9. 500 MHz  ${}^1\text{H}$  NMR spectra at 298 K of  $[\text{Lu}(\text{fod})_3(\text{py-im})]$  in  $\text{CDCl}_3$ . Asterisks are impurities.



**Fig. S10.** Thermogravimetry analysis (TGA) curves of the complexes.



**Fig. S11** Tauc's plot of the complexes.

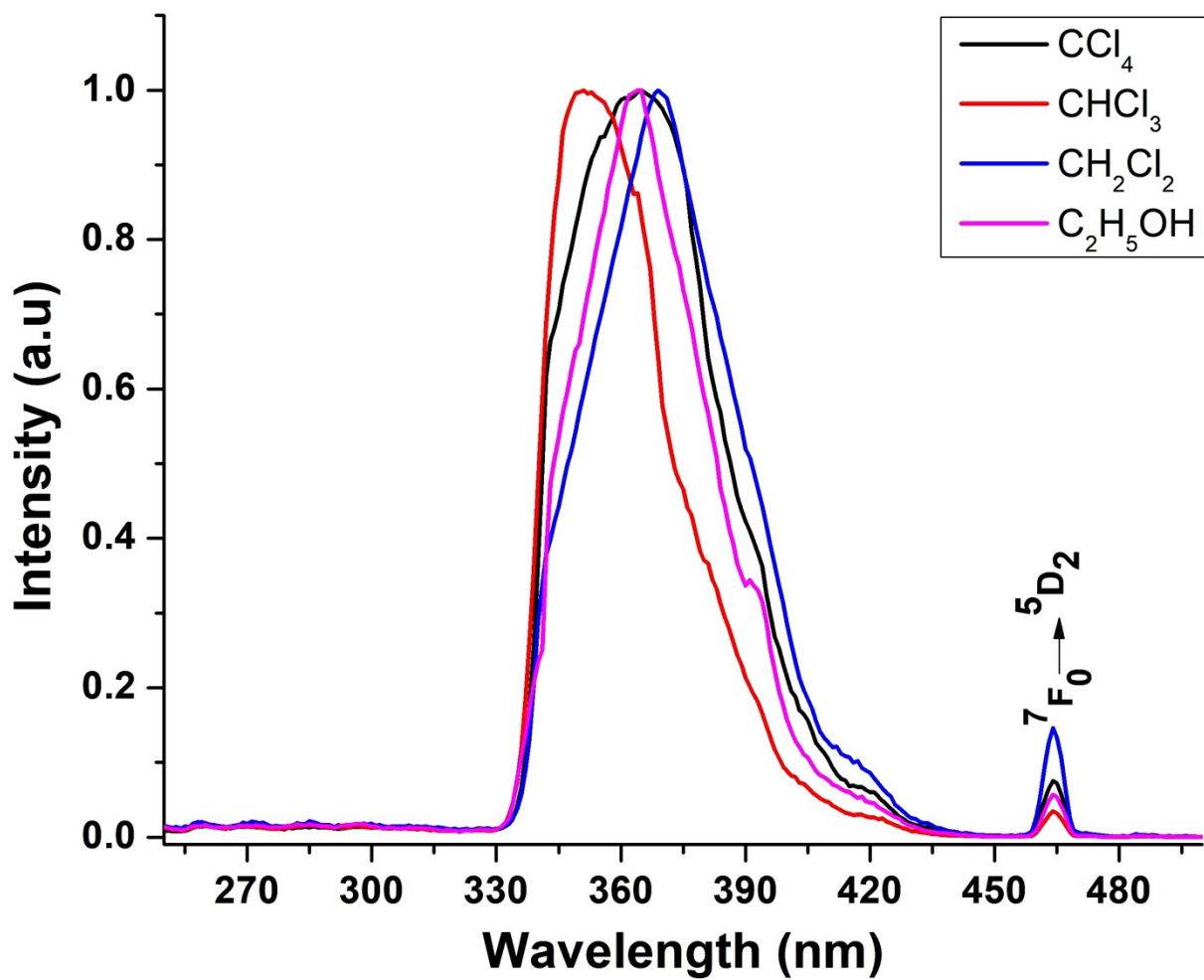


**Fig. S12.** Normalized excitation spectra of complex  $[\text{Eu}(\text{fod})_3(\text{bzi})]$  in different solvents.

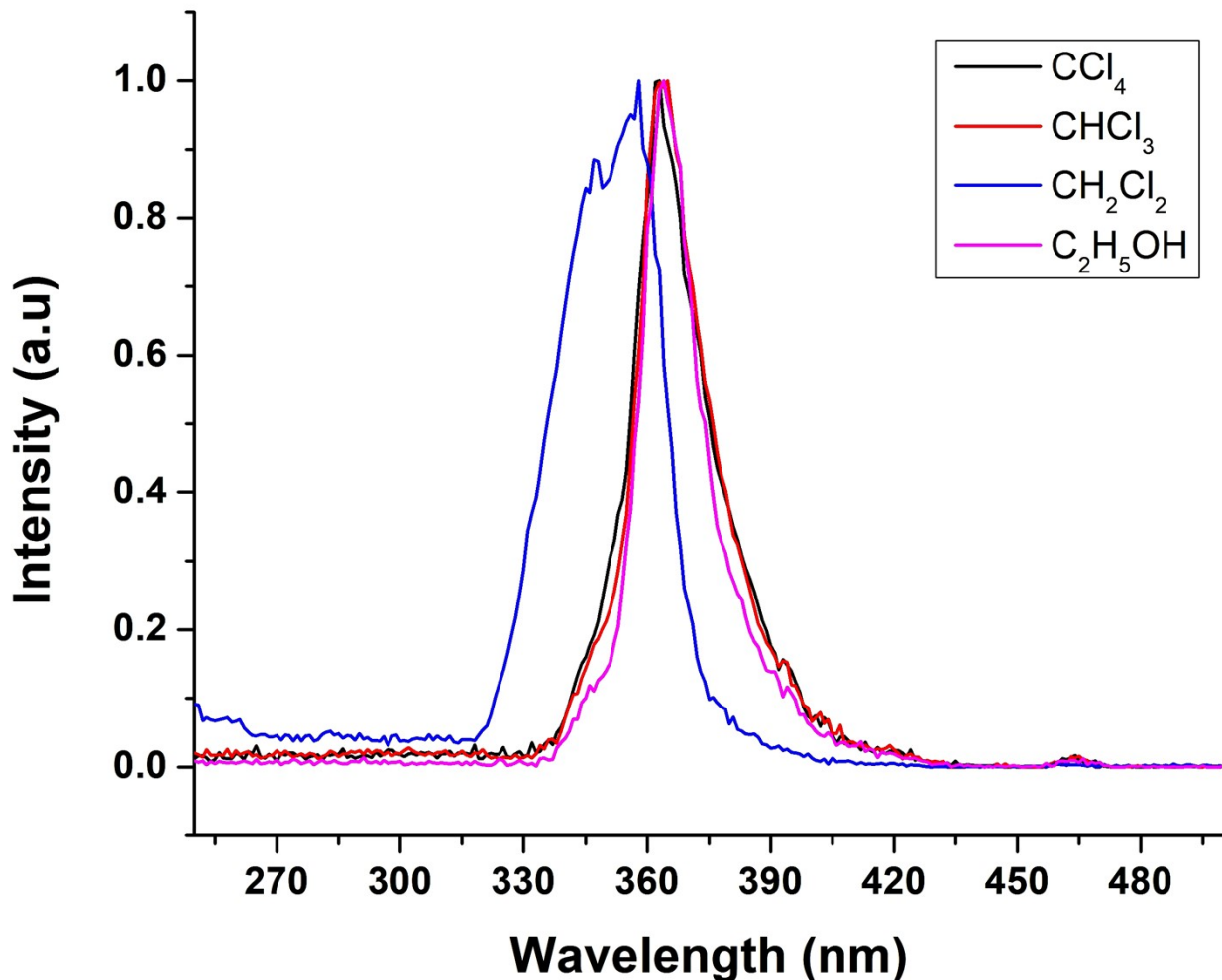


**Fig. S12.** Normalized excitation spectra of complex  $[\text{Eu}(\text{fod})_3(\text{bath})]$  in different solvents.

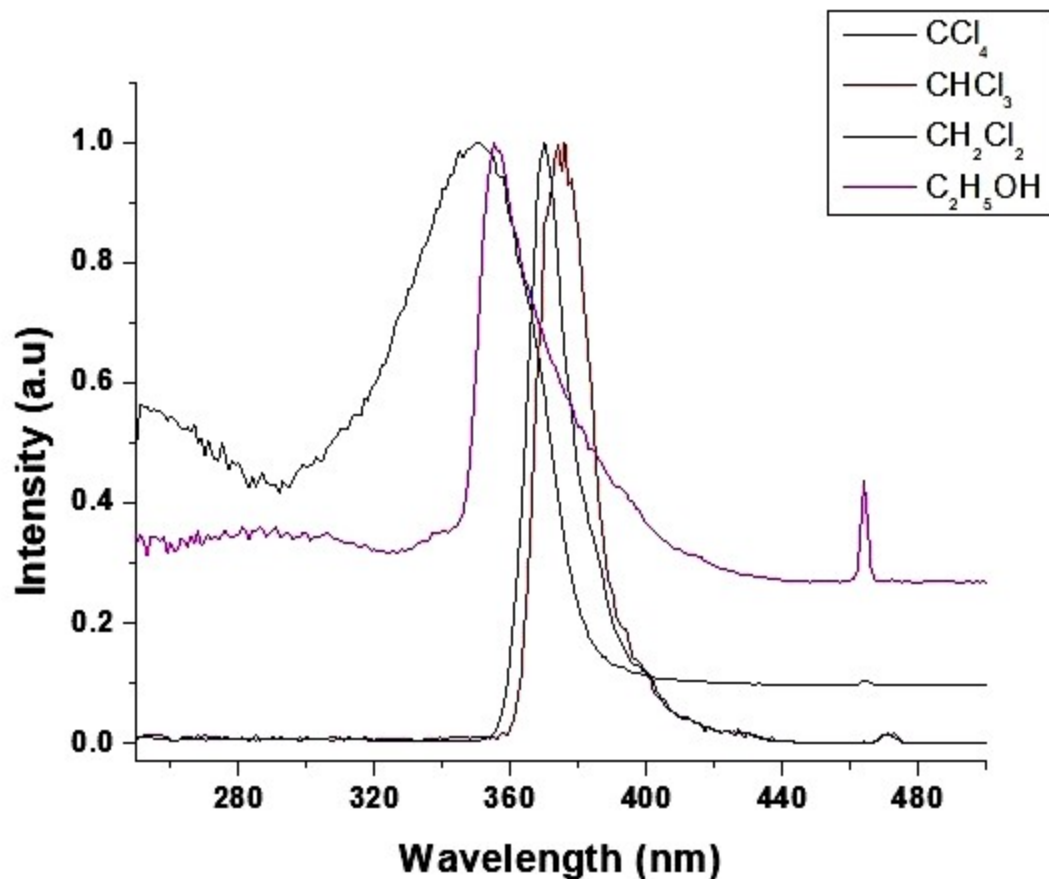


**Fig. S14.** Normalized excitation spectra of complex  $[\text{Eu}(\text{fod})_3(\text{py-im})]$  in different solvents.

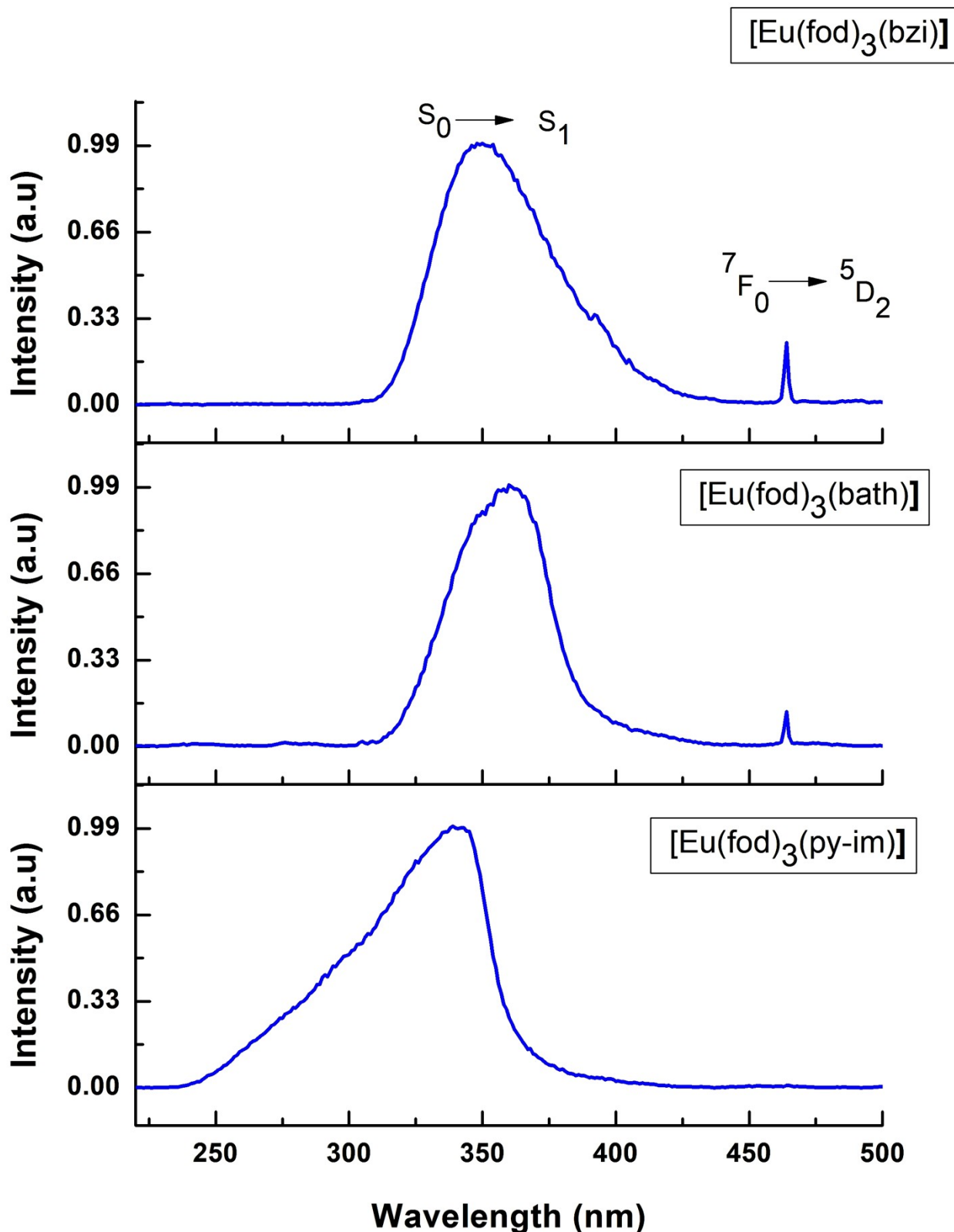


**Fig. S14.** Normalized excitation spectra of complexes in solid state.

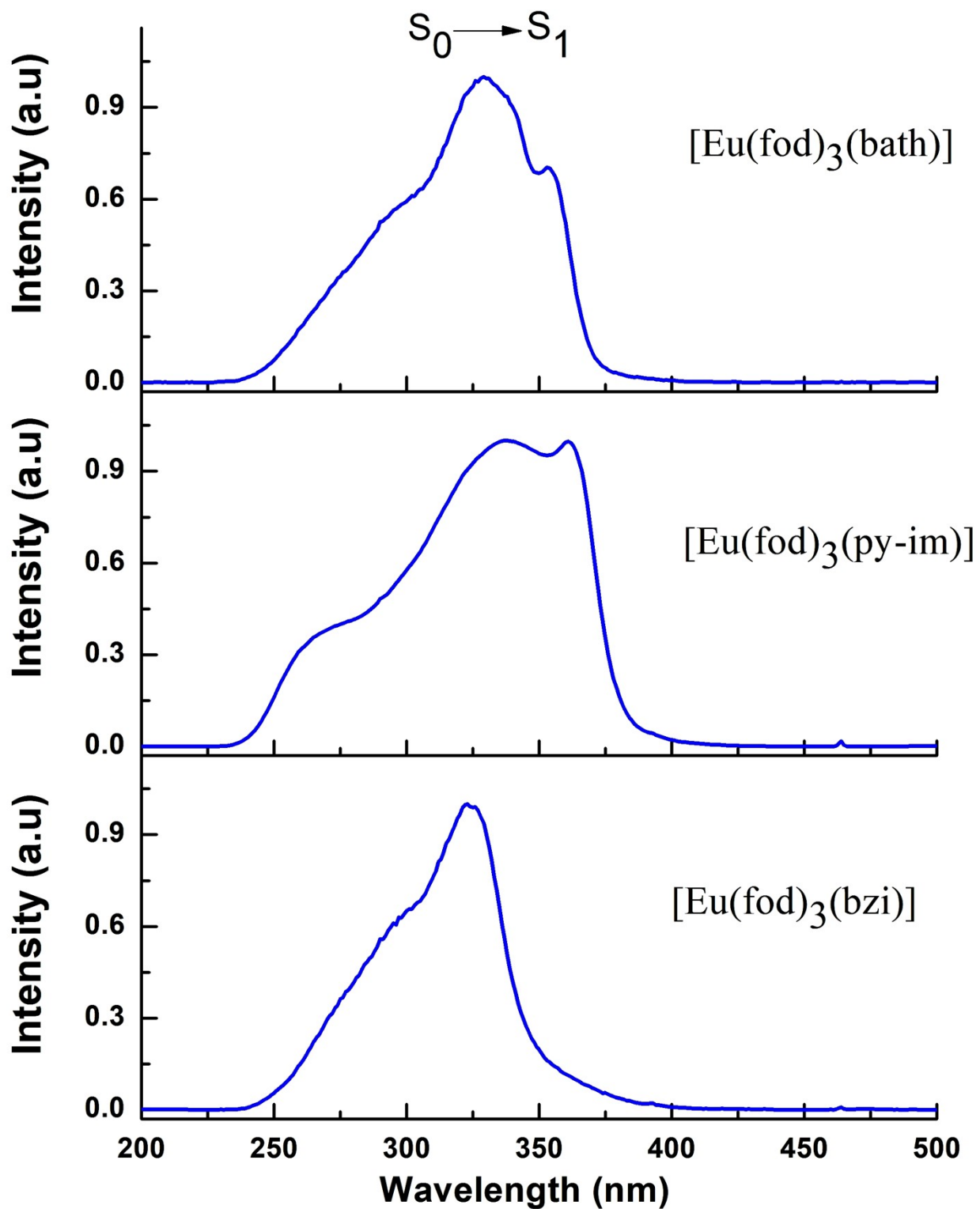


**Fig. S16.** Normalized excitation spectra of complexes in 3% PMMA Thin Film.

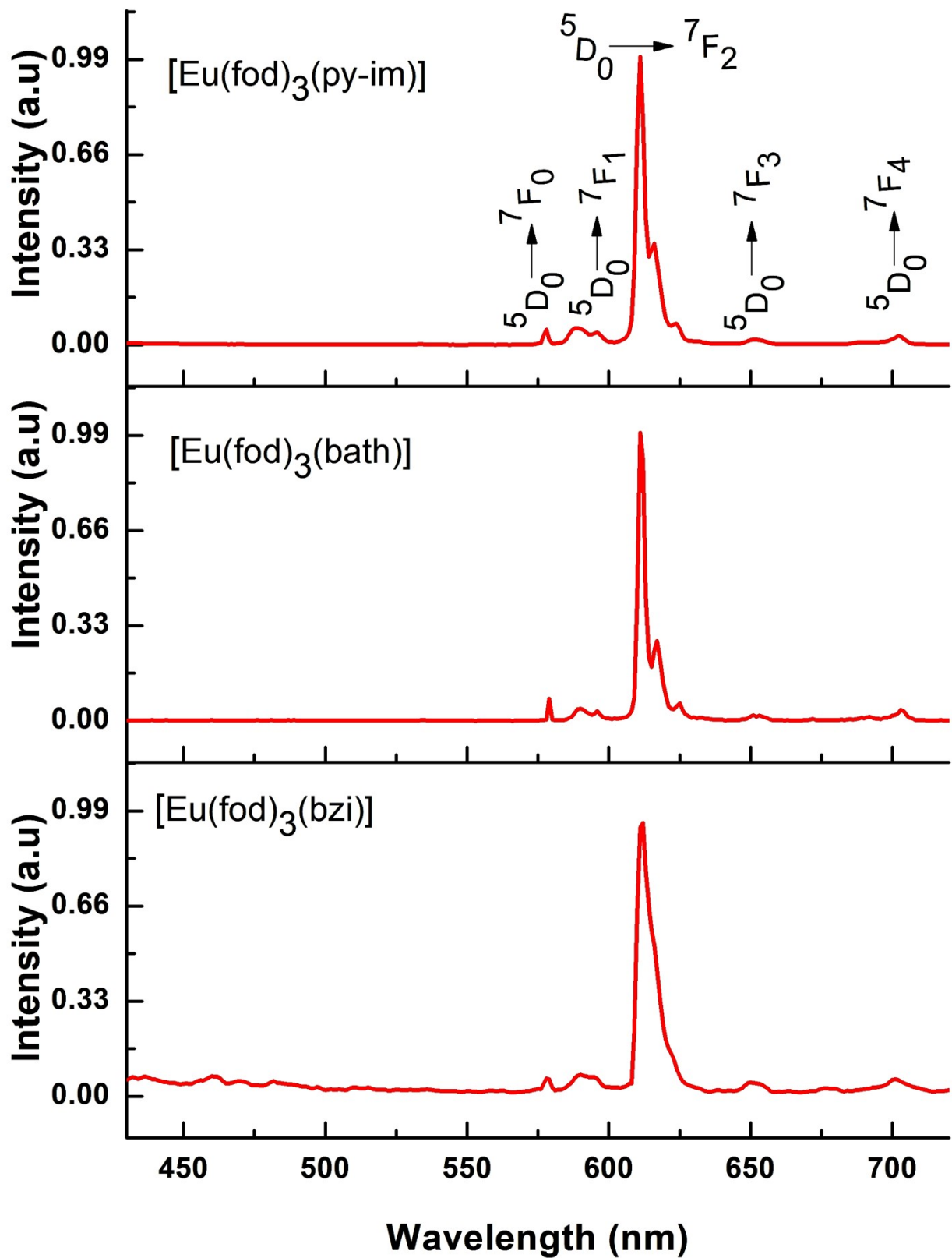


**Fig. S17.** Normalized emission spectra of complexes in 3% PMMA Thin Film.

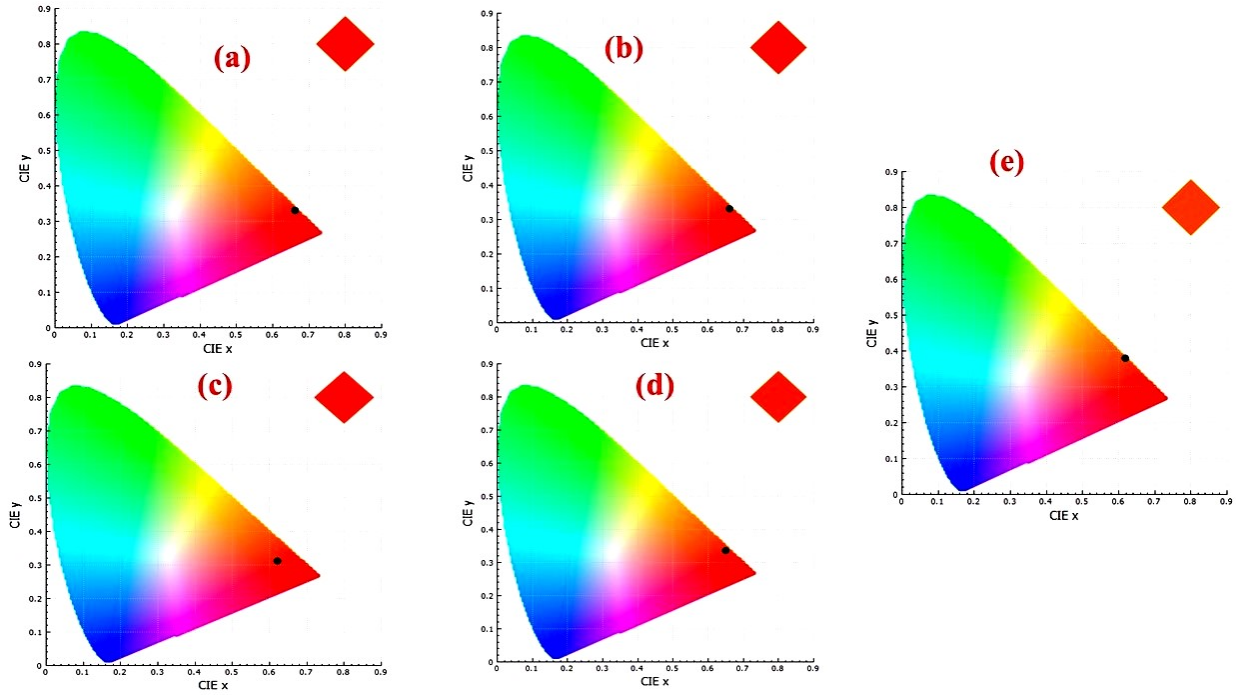


**Fig. S18.** CIE chromaticity diagram of  $\text{Eu}(\text{fod})_3(\text{bzi})$  in (a) Carbon tetrachloride (b) Dichloromethane (c) Ethanol (d) Solid state and (e) 3% PMMA.

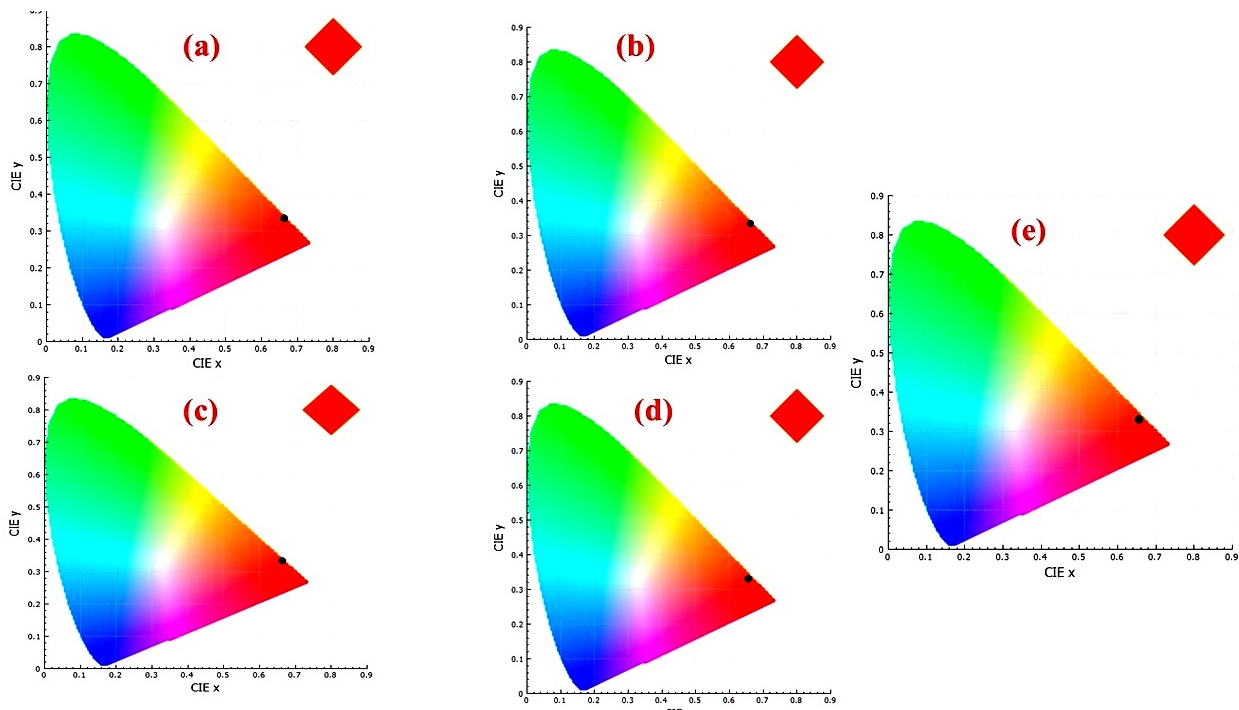


**Fig. S19.** CIE chromaticity diagram of  $\text{Eu}(\text{fod})_3(\text{bath})$  in (a) Carbon tetrachloride (b) Dichloromethane (c) Ethanol (d) Solid state and (e) 3% PMMA.

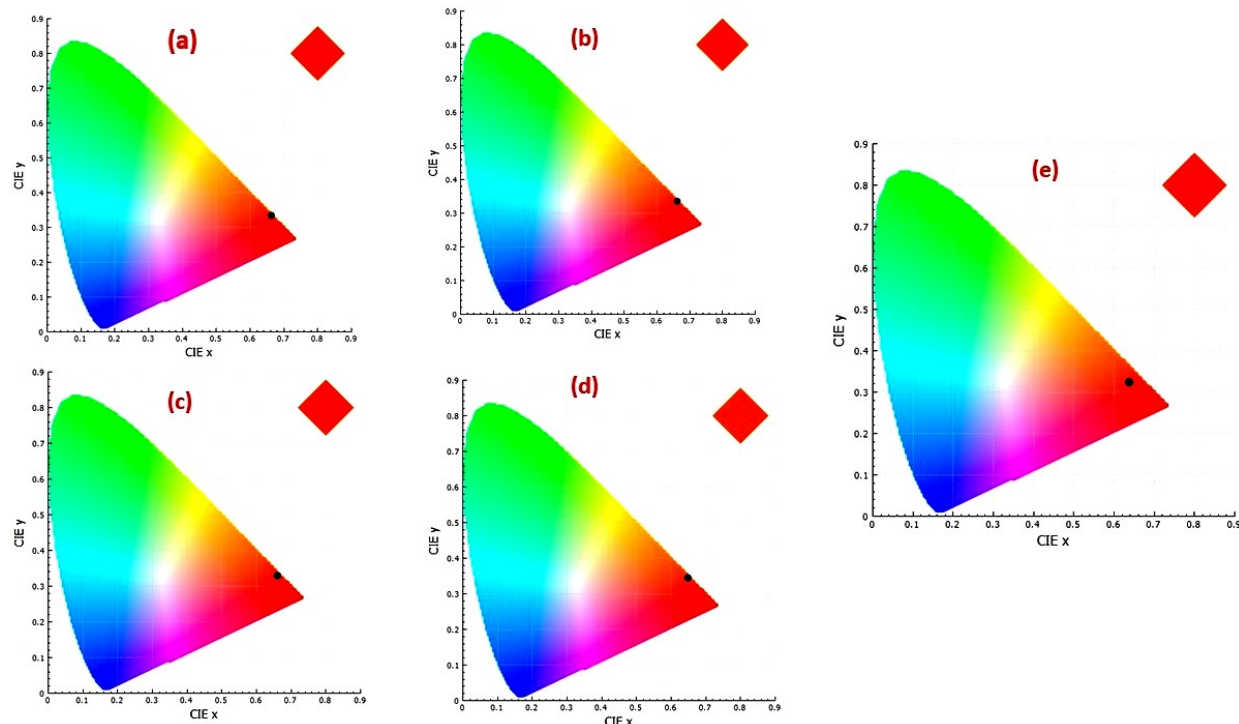


**Fig. S20.** CIE chromaticity diagram of  $\text{Eu}(\text{fod})_3(\text{py-im})$  in (a) Carbon tetrachloride (b) Dichloromethane (c) Ethanol (d) Solid state and (e) 3% PMMA.

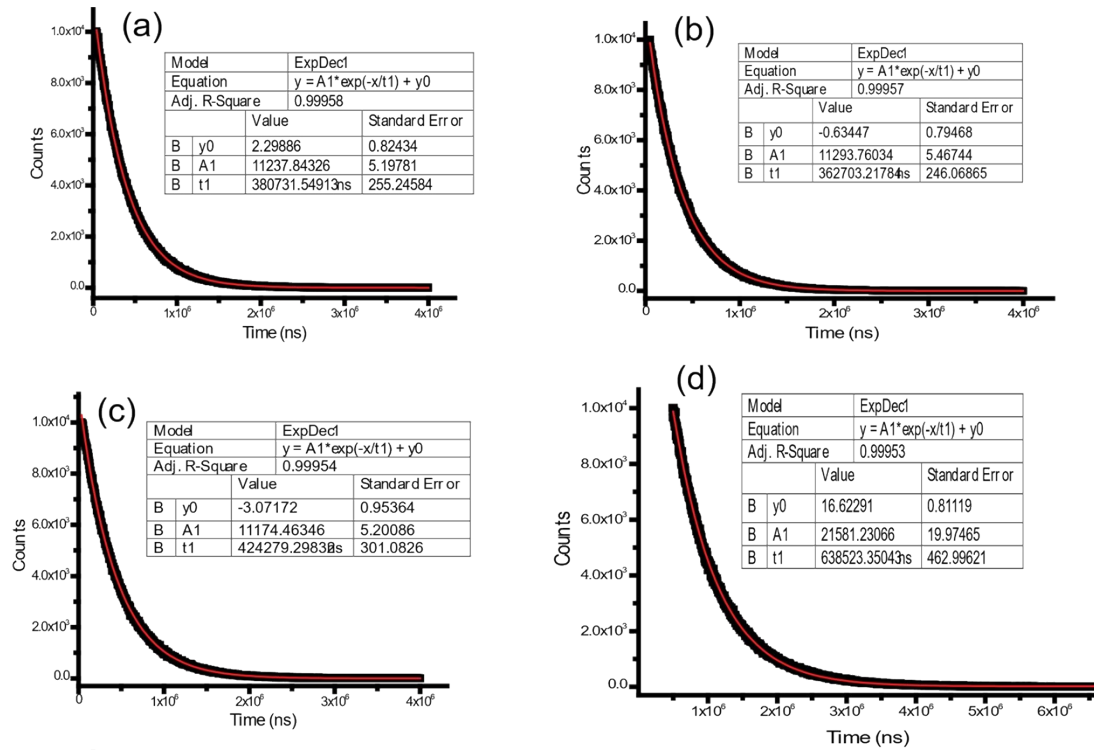


**Fig. S21.** Emission lifetimes of  $\text{Eu}(\text{fod})_3(\text{bzi})$  in (a) Carbon tetrachloride (b) dichloromethane (c) ethanol and (d) 3% PMMA thin film.

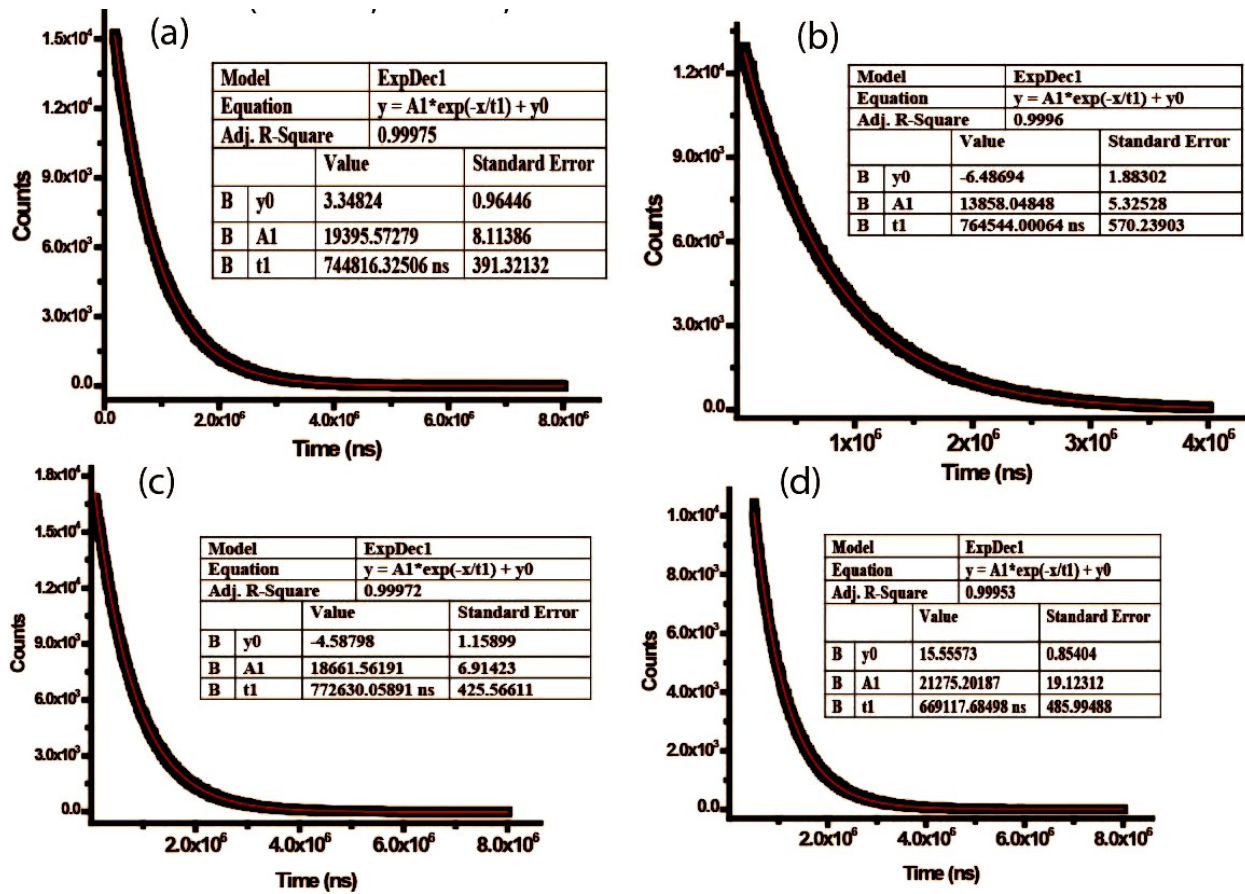


**Fig. S22.** Emission lifetimes of  $\text{Eu}(\text{fod})_3$ (bath) in (a) Carbon tetrachloride (b) dichloromethane (c) ethanol and (d) 3% PMMA thin film.

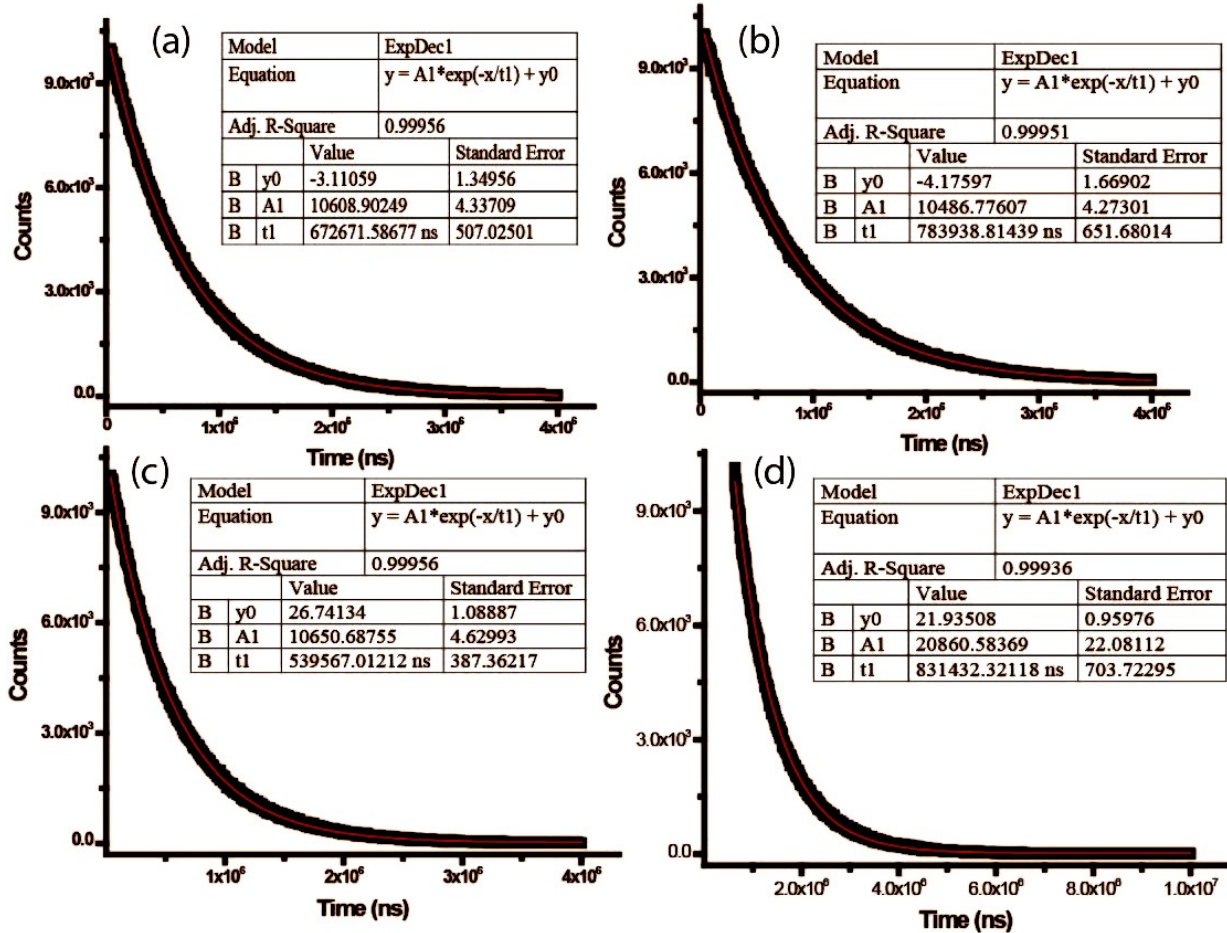


**Fig. S23.** Emission lifetimes of Eu(fod)<sub>3</sub>(py-im) in (a) Carbon tetrachloride (b) dichloromethane (c) ethanol and (d) 3% PMMA thin film.

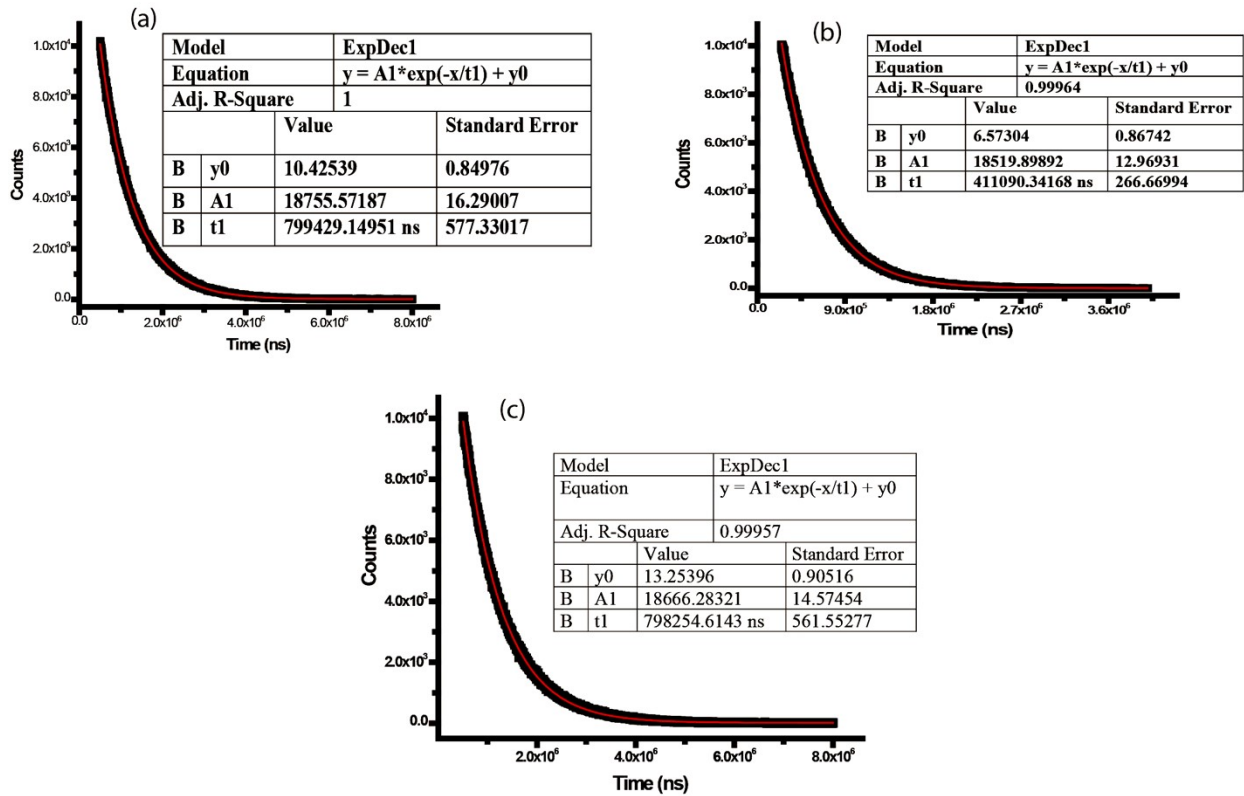


**Fig. S24.** Emission lifetimes of (a) Eu(fod)<sub>3</sub>(bath), (b) Eu(fod)<sub>3</sub>(bzi) and (c) Eu(fod)<sub>3</sub>(py-im) in solid state.

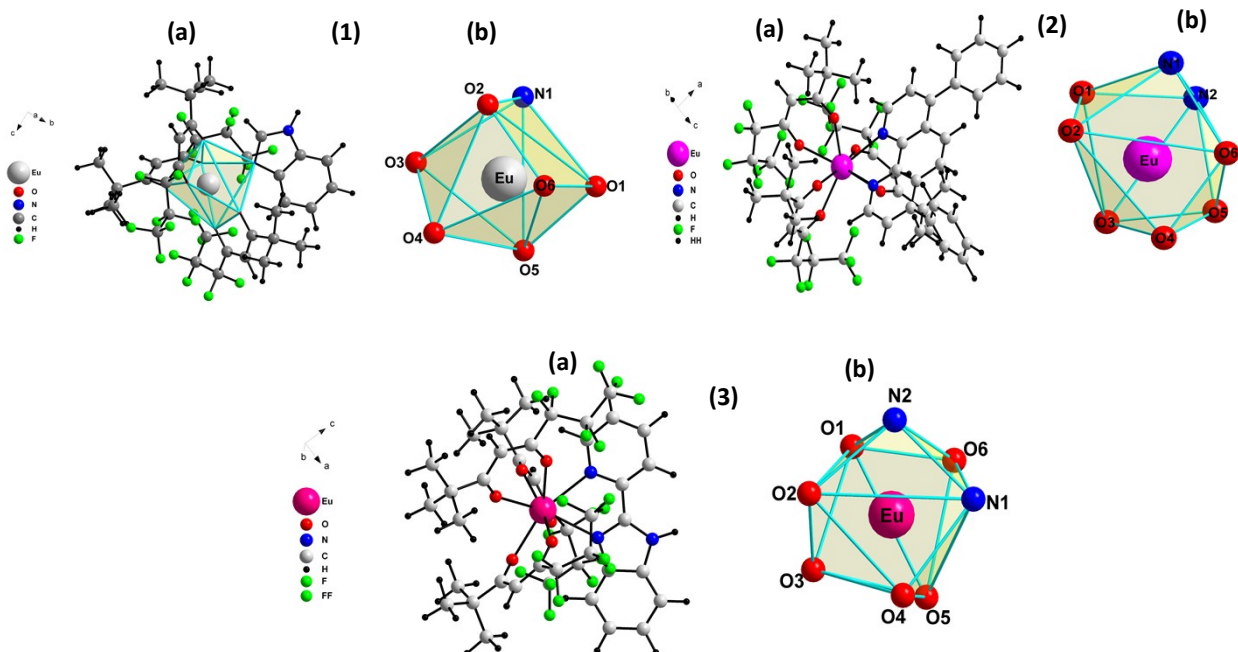


**Fig.S25.** (a) Ground state geometry obtained using Sparkle/PM7 and (b) coordinationpolyhedron around the metal ion of (i) [Eu(fod)<sub>3</sub>(bzi)], (ii) [Eu(fod)<sub>3</sub>(bath)], and (iii) Eu(fod)<sub>3</sub>(py-im)].

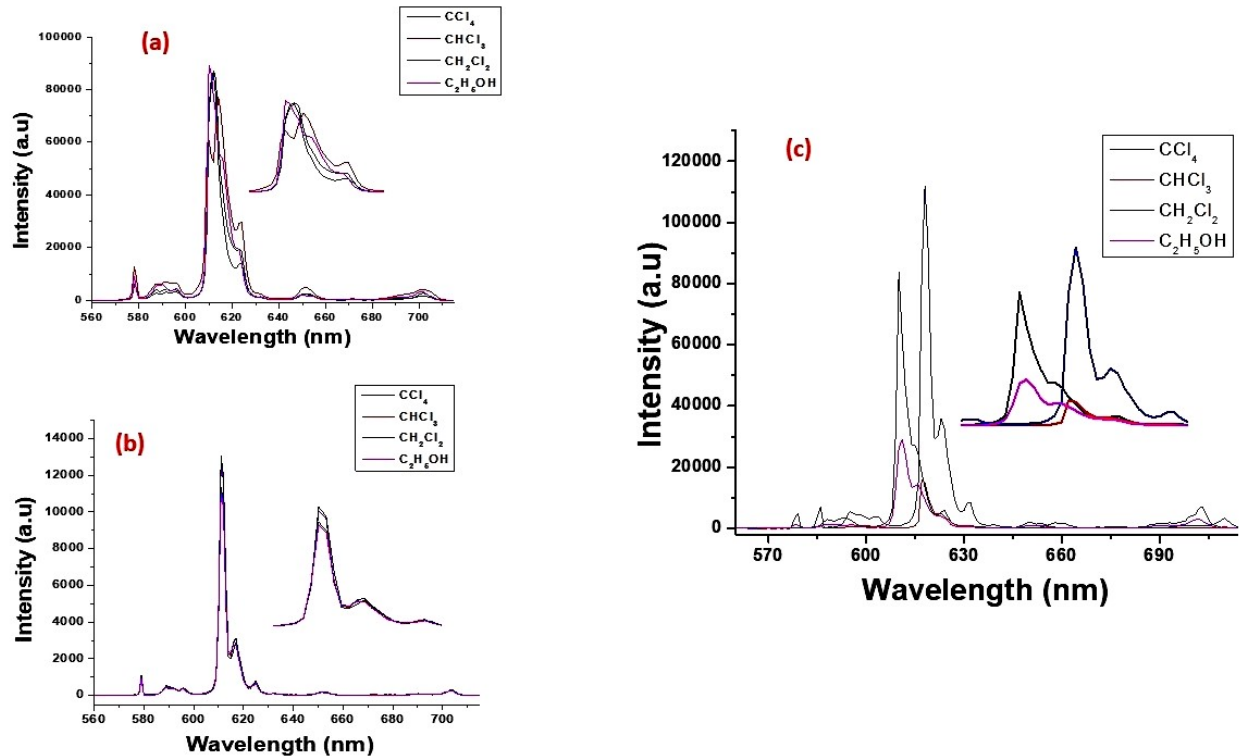


**Figure S26.** Emission spectra of (a) [Eu(fod)<sub>3</sub>(bzi)], (b) [Eu(fod)<sub>3</sub>(bath)] and (c) [Eu(fod)<sub>3</sub>(py-im)] in different solvents.

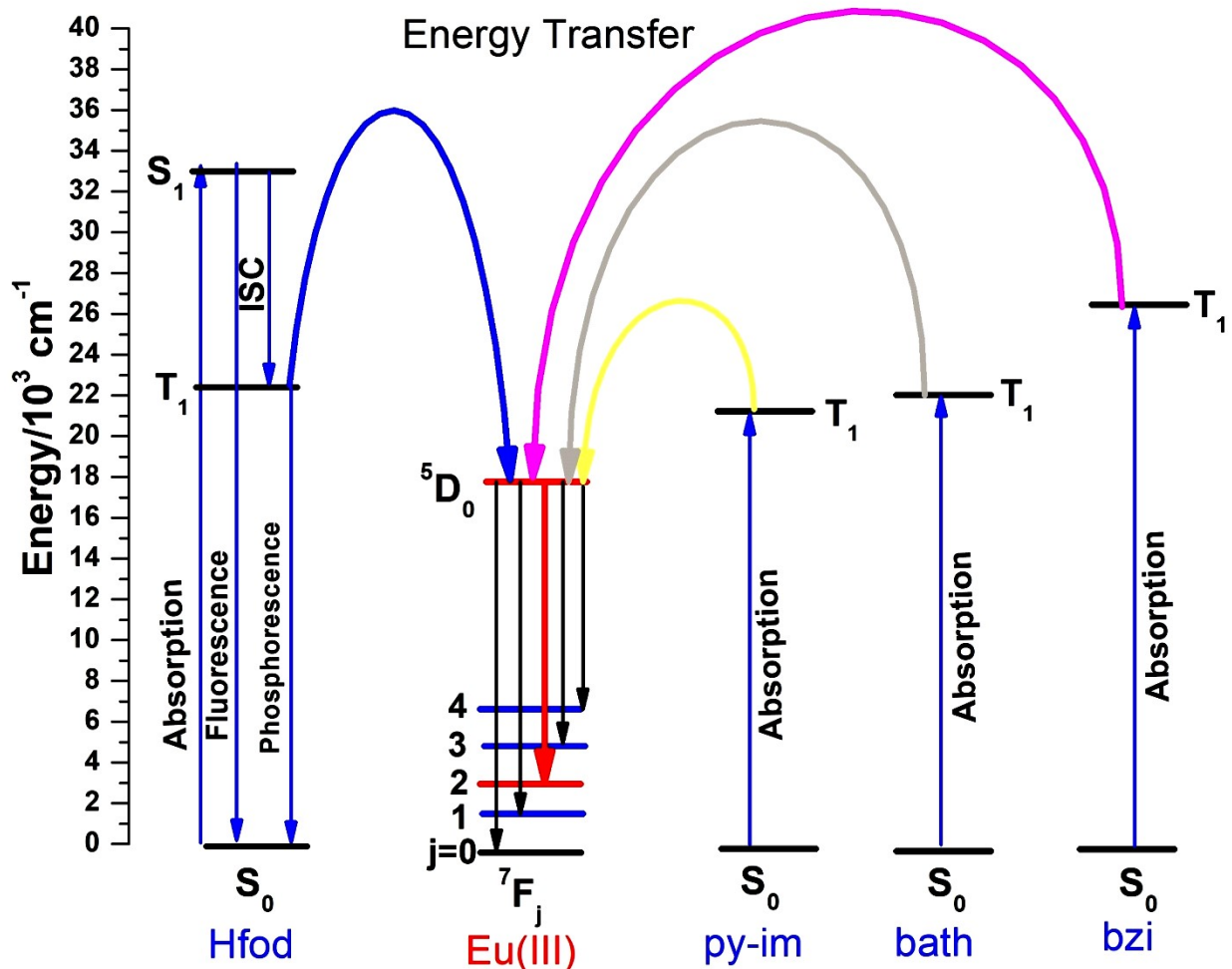


**Figure S27.** The energy level representation shows the triplet state of ligands with respect to the emitting level of Eu(III).

**TableS1.** Selected bond lengths ( $\text{\AA}$ ) and bond angles ( $^\circ$ ) of  $[\text{Eu}(\text{fod})_3(\text{bzi})]$

Eu(1)-O(3)	2.300(4)	O(3)-Eu(1)-O(4)	72.94(14)	O(4)-Eu(1)-O(2)	80.42(15)	O(2)-Eu(1)-O(1)	73.31(12)
Eu(1)-O(4)	2.317(4)	O(3)-Eu(1)-O(6)	122.01(14)	O(6)-Eu(1)-O(2)	145.12(13)	O(3)-Eu(1)-N(1)	78.64(14)
Eu(1)-O(6)	2.325(4)	O(4)-Eu(1)-O(6)	79.34(15)	O(5)-Eu(1)-O(2)	78.50(15)	O(4)-Eu(1)-N(1)	123.04(15)
Eu(1)-O(5)	2.340(4)	O(3)-Eu(1)-O(5)	150.59(15)	O(3)-Eu(1)-O(1)	105.07(13)	O(6)-Eu(1)-N(1)	75.61(13)
Eu(1)-O(2)	2.350(4)	O(4)-Eu(1)-O(5)	86.14(14)	O(4)-Eu(1)-O(1)	153.36(16)	O(5)-Eu(1)-N(1)	130.70(15)
Eu(1)-O(1)	2.372(3)	O(6)-Eu(1)-O(5)	72.08(14)	O(6)-Eu(1)-O(1)	120.78(13)	O(2)-Eu(1)-N(1)	139.16(13)

Eu(1)-N(1)	2.497(4)	O(3)-Eu(1)-O(2)	77.82(14)	O(5)-Eu(1)-O(1)	84.39(12)	O(1)-Eu(1)-N(1)	81.28(13)
------------	----------	-----------------	-----------	-----------------	-----------	-----------------	-----------

**Table S2.** Selected bond lengths of Eu(fod)<sub>3</sub>(bath) complex.

Unit 1		Unit 2	
Eu(1)-O(1)	2.381(2)	Eu(2)-O(7)	2.361(2)
Eu(1)-O(2)	2.353(2)	Eu(2)-O(8)	2.362(2)
Eu(1)-O(3)	2.343(2)	Eu(2)-O(9)	2.403(2)
Eu(1)-O(4)	2.368(2)	Eu(2)-O(10)	2.357(3)
Eu(1)-O(5)	2.354(2)	Eu(2)-O(11)	2.359(2)
Eu(1)-O(6)	2.371(2)	Eu(2)-O(12)	2.357(3)
Eu(1)-N(1)	2.593(3)	Eu(2)-N(3)	2.574(3)
Eu(1)-N(2)	2.580(3)	Eu(2)-N(4)	2.570(3)

**TableS3.** Selected bond angles (°) for [Eu(fod)<sub>3</sub>(bath)] complex.

Unit 1				Unit 2			
O(1)-Eu(1)-N(1)	122.12(8)	O(3)-Eu(1)-N(2)	147.11(8)	O(7)-Eu(2)-O(8)	71.84(8)	O(10)-Eu(2)-N(3)	113.31(10)
O(1)-Eu(1)-N(2)	74.17(8)	O(4)-Eu(1)-O(1)	134.55(8)	O(7)-Eu(2)-O(9)	77.77(9)	O(10)-Eu(2)-N(4)	71.41(9)
O(2)-Eu(1)-O(1)	70.64(8)	O(4)-Eu(1)-O(6)	130.20(8)	O(7)-Eu(2)-N(3)	78.55(9)	O(11)-Eu(2)-O(7)	121.37(9)
O(2)-Eu(1)-O(4)	77.92(9)	O(4)-Eu(1)-N(1)	78.65(8)	O(7)-Eu(2)-N(4)	138.22(9)	O(11)-Eu(2)-O(8)	79.32(8)
O(2)-Eu(1)-O(5)	142.53(8)	O(4)-Eu(1)-N(2)	141.22(8)	O(8)-Eu(2)-O(9)	78.55(9)	O(11)-Eu(2)-O(9)	143.66(8)
O(2)-Eu(1)-O(6)	145.78(8)	O(5)-Eu(1)-O(1)	144.32(8)	O(8)-Eu(2)-N(3)	146.79(9)	O(11)-Eu(2)-N(3)	130.39(9)
O(2)-Eu(1)-N(1)	75.73(8)	O(5)-Eu(1)-O(4)	77.60(8)	O(8)-Eu(2)-N(4)	149.64(8)	O(11)-Eu(2)-N(4)	78.92(9)

O(2)-Eu(1)-N(2)	94.02(8)	O(5)-Eu(1)-O(6)	70.52(8)	O(9)-Eu(2)-N(3)	80.83(9)	O(12)-Eu(2)-O(7)	74.95(9)
O(3)-Eu(1)-O(1)	76.26(8)	O(5)-Eu(1)-N(1)	71.96(8)	O(9)-Eu(2)-N(4)	107.99(9)	O(12)-Eu(2)-O(8)	112.67(10)
O(3)-Eu(1)-O(2)	89.49(9)	O(5)-Eu(1)-N(2)	87.70(8)	O(10)-Eu(2)-O(7)	143.20(9)	O(12)-Eu(2)-O(9)	144.87(8)
O(3)-Eu(1)-O(4)	71.41(8)	O(6)-Eu(1)-O(1)	75.16(8)	O(10)-Eu(2)-O(8)	83.76(9)	O(12)-Eu(2)-O(11)	70.92(8)
O(3)-Eu(1)-O(5)	108.83(9)	O(6)-Eu(1)-N(1)	123.46(8)	O(10)-Eu(2)-O(9)	70.53(9)	O(12)-Eu(2)-N(3)	72.45(9)
O(3)-Eu(1)-O(6)	83.77(8)	O(6)-Eu(1)-N(2)	75.08(8)	O(10)-Eu(2)-O(11)	78.72(9)	O(12)-Eu(2)-N(4)	79.50(9)
O(3)-Eu(1)-N(1)	148.83(8)	N(2)-Eu(1)-N(1)	62.65(8)	O(10)-Eu(2)-O(12)	141.28(8)	N(4)-Eu(2)-N(3)	62.37(9)

**Table S4.** Selected bond lengths (Å) and bond angles (°) of [Eu(fod)<sub>3</sub>(py-im)]

Eu(1)-O(3)	2.3485(18)	O(3)-Eu(1)-O(4)	71.82(6)	O(4)-Eu(1)-O(2)	79.74(6)	O(2)-Eu(1)-O(1)	69.97(6)
Eu(1)-O(4)	2.3802(18)	O(3)-Eu(1)-O(6)	78.66(6)	O(6)-Eu(1)-O(2)	142.38(6)	O(3)-Eu(1)-N(1)	147.62(6)
Eu(1)-O(6)	2.3760(17)	O(4)-Eu(1)-O(6)	131.98(6)	O(5)-Eu(1)-O(2)	146.52(6)	O(4)-Eu(1)-N(1)	75.94(6)
Eu(1)-O(5)	2.3447(18)	O(3)-Eu(1)-O(5)	92.55(7)	O(3)-Eu(1)-O(1)	75.33(6)	O(6)-Eu(1)-N(1)	123.06(7)
Eu(1)-O(2)	2.4110(17)	O(4)-Eu(1)-O(5)	73.52(6)	O(4)-Eu(1)-O(1)	131.06(6)	O(5)-Eu(1)-N(1)	75.40(7)
Eu(1)-O(1)	2.4371(18)	O(6)-Eu(1)-O(5)	70.86(6)	O(6)-Eu(1)-O(1)	73.00(6)	O(2)-Eu(1)-N(1)	78.89(6)
Eu(1)-N(1)	2.645(2)	O(3)-Eu(1)-O(2)	97.94(6)	O(5)-Eu(1)-O(1)	143.49(6)	O(1)-Eu(1)-N(1)	130.99(6)

Eu(1)-N(2)	2.529(2)	O(3)-Eu(1)-N(2)	148.78(6)	O(2)-Eu(1)-N(2)	90.46(6)	O(1)-Eu(1)-N(2)	79.54(6)
O(4)-Eu(1)-N(2)	139.40(6)	O(5)-Eu(1)-N(2)	96.83(7)	O(6)-Eu(1)-N(2)	76.48(6)	N(1)-Eu(1)-N(2)	63.50(7)

**Table S5.**Spherical coordinates of the coordination polyhedron, Charge factor (g) and polarizability ( $\alpha$ ) for Sparkle/PM7 optimized structure of [Eu(fod)<sub>3</sub>(bzi)] complex.

PM7	R (Å)	(θ)°	(Φ)°	Charge factor (g)	Polarizability ( $\alpha$ )
Eu	0.0000	0.00	0.00	-	-
O(fod)	2.3860	135.77	215.97	1.0177	1.0364
O(fod)	2.3662	76.83	187.96	1.0155	1.2269
O(fod)	2.3700	78.68	103.23	1.0151	5.2522
O(fod)	2.3742	45.93	38.65	1.0209	4.7169
O(fod)	2.3627	61.56	279.41	1.0179	0.4519
O(fod)	2.3728	110.45	322.72	1.0174	0.0072
N(bzi)	2.5031	144.98	64.82	0.8438	5.8854

**Table S6.**Spherical coordinates of the coordination polyhedron, Charge factor (g) and polarizability ( $\alpha$ ) for Sparkle/PM7 optimized structure of [Eu(fod)<sub>3</sub>(bath)] complex.

<b>PM7</b>	<b>R (Å)</b>	<b>(θ)°</b>	<b>(Φ)°</b>	<b>Charge factor (g)</b>	<b>Polarizability (<math>\alpha</math>)</b>
Eu	0.00000	0.00	0.00	-	-
O(fod)	2.39176	77.794	199.492	1.2430	1.1482
O(fod)	2.38528	73.053	133.078	1.2395	0.7539
O(fod)	2.38386	115.716	60.258	1.2401	0.0054
O(fod)	2.39723	149.126	142.644	1.2392	1.2883
O(fod)	2.40249	54.597	293.902	1.2352	1.3784
O(fod)	2.36755	118.152	301.676	1.2457	1.4247
N(bath)	2.54739	22.081	53.557	1.0072	8.7023
N(bath)	2.54904	78.825	4.824	1.0035	9.0190

**Table S7.**Spherical coordinates of the coordination polyhedron, Charge factor (g) and polarizability ( $\alpha$ ) for Sparkle/PM7 optimized structure of [Eu(fod)<sub>3</sub>(py-im)] complex.

PM7	R (Å)	(θ)°	(Φ)°	Charge factor (g)	Polarizability ( $\alpha$ )
Eu	0.00000	0.00	0.00	-	-
O(fod)	2.40296	111.462	315.510	0.7073	0.0074
O(fod)	2.38066	156.043	31.637	0.7091	0.2642
O(fod)	2.38392	76.201	152.527	0.7089	0.8661
O(fod)	2.40020	78.041	87.133	0.7090	0.4338
O(fod)	2.38057	129.118	222.902	0.7089	0.6238
O(fod)	2.39494	66.794	237.639	0.7083	1.0039
N(py-im)	2.51605	62.071	8.153	0.5830	5.5715
N(py-im)	2.56340	2.428	155.818	0.5732	6.2288

**Table S8.** SHAPE measured deviations from ideal seven coordinate geometries of [Eu(fod)<sub>3</sub>(bzi)] complex.

S. No.	SHAPE	Symmetry	Deviation
1	Heptagon	D <sub>7h</sub>	35.001
2	Hexagonal pyramid	C <sub>6v</sub>	19.544
3	Pentagonal bipyramid	D <sub>5h</sub>	6.684
4	Capped octahedron	C <sub>3v</sub>	<b>0.789</b>
5	Capped trigonal prism	C <sub>2v</sub>	1.005
6	Johnson pentagonal bipyramid J13	D <sub>5h</sub>	10.092
7	Johnson elongated triangular pyramid J7	C <sub>3v</sub>	18.111

**TableS9.** SHAPE measured deviations from ideal eight coordinate geometries of  $[\text{Eu}(\text{fod})_3(\text{bath})]$  and  $[\text{Eu}(\text{fod})_3(\text{py-im})]$  complex.

S. No.	SHAPE	Symmetry	Deviation $[\text{Eu}(\text{fod})_3(\text{bath})]$	Deviation $[\text{Eu}(\text{fod})_3(\text{py-im})]$
1	Octagon	$D_{8h}$	31.178	32.505
2	Heptagonal pyramid	$C_{7v}$	23.416	23.565
3	Hexagonal bipyramid	$D_{6h}$	15.189	16.668
4	Cube	$O_h$	9.009	10.088
5	Square antiprism	$D_{4d}$	2.008	2.408
6	Triangular dodecahedron	$D_{2d}$	<b>0.580</b>	<b>0.559</b>
7	Johnson gyrobifastigium J26	$D_{2d}$	14.632	13.237
8	Johnson elongated triangular bipyramid J14	$D_{3h}$	28.680	29.314
9	Biaugmented trigonal prism J50	$C_{2v}$	2.497	2.966
10	Biaugmented trigonal prism	$C_{2v}$	1.888	2.309
11	Snub diphenoïd J84	$D_{2d}$	3.255	2.788
12	Triakis tetrahedron	$T_d$	9.693	10.682
13	Elongated trigonal bipyramid	$D_{3h}$	23.350	25.245

**Table S10.** SHAPE measured deviations from ideal seven coordinate geometries in Sparkle/PM7 predicted [Eu(fod)<sub>3</sub>(bzi)] complex.

S. No.	SHAPE	Symmetry	Deviation [Eu(fod) <sub>3</sub> (bzi)]
1	Heptagon	D <sub>7h</sub>	350259
2	Hexagonal pyramid	C <sub>6v</sub>	17.862
3	Pentagonal bipyramid	D <sub>5h</sub>	6.305
4	Capped octahedron	C <sub>3v</sub>	2.977
5	Capped trigonal prism	C <sub>2v</sub>	<b>2.528</b>
6	Johnson pentagonal bipyramid J13	D <sub>5h</sub>	10.288
7	Johnson elongated triangular pyramid J7	C <sub>3v</sub>	19.040

**Table S11.** SHAPE measured deviations from ideal seven coordinate geometries in Sparkle/PM7 predicted [Eu(fod)<sub>3</sub>(bath)] and [Eu(fod)<sub>3</sub>(py-im)] complex.

S. No.	SHAPE	Symmetry	Deviation [Eu(fod) <sub>3</sub> (bath)]	Deviation [Eu(fod) <sub>3</sub> (py-im)]
1	Octagon	D <sub>8h</sub>	30.337	28.622
2	Heptagonal pyramid	C <sub>7v</sub>	20.969	21.579
3	Hexagonal bipyramid	D <sub>6h</sub>	15.023	13.316
4	Cube	O <sub>h</sub>	8.252	7.330
5	Square antiprism	D <sub>4d</sub>	3.750	2.459
6	Triangular dodecahedron	D <sub>2d</sub>	<b>1.454</b>	<b>2.412</b>
7	Johnson gyrobifastigium J26	D <sub>2d</sub>	14.843	12.200
8	Johnson elongated triangular bipyramid J14	D <sub>3h</sub>	26.072	24.813
9	Biaugmented trigonal prism J50	C <sub>2v</sub>	4.503	4.120
10	Biaugmented trigonal prism	C <sub>2v</sub>	3.701	3.617
11	Snub diphenoïd J84	D <sub>2d</sub>	4.388	5.562
12	Triakis tetrahedron	T <sub>d</sub>	8.797	8.108
13	Elongated trigonal bipyramid	D <sub>3h</sub>	21.825	20.768

**Table S12.** Experimental Intensity parameters of Eu(fod)<sub>3</sub>(bzi) in different solvents.

Eu(fod) <sub>3</sub> (BZI)	$\Omega_2$ ( $10^{-20} cm^2$ )	$\Omega_4$ ( $10^{-20} cm^2$ )	$\tau_{obs}$ ( $\mu s$ )	$\tau_{rad}$ ( $\mu s$ )	$A_{rad}$ ( $s^{-1}$ )	$A_{nrad}$ ( $s^{-1}$ )	$\phi_{Eu}^{Eu}$ %	R	Color coordinates (x, y)
CCl <sub>4</sub>	23.45	1.39	380	1347.83	741.93	1884.81	28.25	13.34	0.639, 0.340
CH <sub>2</sub> Cl <sub>2</sub>	28.06	1.41	362	1242.37	804.91	1952.19	29.19	16.00	0.661, 0.338
C <sub>2</sub> H <sub>5</sub> OH	21.70	1.61	424	1790.63	558.46	1798.92	23.69	12.33	0.629, 0.314

**Table S13.** Experimental Intensity parameters of [Eu(fod)<sub>3</sub>(bath)] in different solvents.

Eu(fod) <sub>3</sub> (bath)	$\Omega_2$ ( $10^{-20} cm^2$ )	$\Omega_4$ ( $10^{-20} cm^2$ )	$\tau_{obs}$ ( $\mu s$ )	$\tau_{rad}$ ( $\mu s$ )	$A_{rad}$ ( $s^{-1}$ )	$A_{nrad}$ ( $s^{-1}$ )	$\phi_{Eu}^{Eu}$ %	R	Color coordinates (x, y)
-----------------------------	-----------------------------------	-----------------------------------	-----------------------------	-----------------------------	---------------------------	----------------------------	--------------------	---	-----------------------------

CCl <sub>4</sub>	23.45	1.36	744	1351.4	739.92	602.72	55.11	13.45	0.663, 0.340
CH <sub>2</sub> Cl <sub>2</sub>	23.47	1.39	764	1456.09	686.77	621.27	52.50	13.46	0.661, 0.338
C <sub>2</sub> H <sub>5</sub> OH	23.43	1.31	772	1679.45	595.43	698.90	46.00	13.45	0.663, 0.338

**Table S14.** Experimental Intensity parameters of Eu(fod)<sub>3</sub>(Py-Im) in different solvents.

Eu(fod) <sub>3</sub> (py-im)	$\Omega_2$ ( $10^{-20} \text{ cm}^2$ )	$\Omega_4$ ( $10^{-20} \text{ cm}^2$ )	$\tau_{obs}$ ( $\mu\text{s}$ )	$\tau_{rad}$ ( $\mu\text{s}$ )	$A_{rad}$ ( $\text{s}^{-1}$ )	$A_{nrad}$ ( $\text{s}^{-1}$ )	$\phi_{Eu}^{Eu} \%$	R	Color coordinates (x, y)
CCl <sub>4</sub>	23.58	5.68	672	1230.86	812.44	674.33	54.64	13.57	0.663, 0.343
CH <sub>2</sub> Cl <sub>2</sub>	20.60	1.22	783	1662.45	601.52	674.15	47.15	11.81	0.659, 0.338
C <sub>2</sub> H <sub>5</sub> OH	25.63	7.58	539	1381.65	723.77	1129.80	39.05	14.64	0.657, 0.335

## References

- (1) Opelt, G. S. Intensities of Crystal Spectra of Rare-Earth Ions. *J. Chem. Phys.* **1962**, *37* (3), 511–520. <https://doi.org/10.1063/1.1701366>.
- (2) Judd, B. R. Optical Absorption Intensities of Rare-Earth Ions. *Phys. Rev.* **1962**, *127* (3), 750–761. <https://doi.org/10.1103/PhysRev.127.750>.
- (3) Werts, M. H. V.; Jukes, R. T. F.; Verhoeven, J. W. The Emission Spectrum and the Radiative Lifetime of Eu<sup>3+</sup> in Luminescent Lanthanide Complexes. *Phys. Chem. Chem. Phys.* **2002**, *4* (9), 1542–1548. <https://doi.org/10.1039/b107770h>.
- (4) Carnall, W. T.; Crosswhite, H.; Crosswhite, H. M. *Energy Level Structure and Transition Probabilities in the Spectra of the Trivalent Lanthanides in LaF<sub>3</sub>*; Argonne, IL (United States), 1978. <https://doi.org/10.2172/6417825>.
- (5) Carnall, W. T.; Fields, P. R.; Rajnak, K. Electronic Energy Levels of the Trivalent Lanthanide Aquo Ions. IV. Eu<sup>3+</sup>. *J. Chem. Phys.* **1968**, *49* (10), 4450–4455. <https://doi.org/10.1063/1.1669896>.
- (6) Kodaira, C. A.; Brito, H. F.; Malta, O. L.; Serra, O. A. Luminescence and Energy Transfer of the

- Europium (III) Tungstate Obtained via the Pechini Method. *J. Lumin.* **2003**, *101* (1–2), 11–21. [https://doi.org/10.1016/S0022-2313\(02\)00384-8](https://doi.org/10.1016/S0022-2313(02)00384-8).
- (7) Ferhi, M.; Bouzidi, C.; Horchani-Naifer, K.; Elhouichet, H.; Ferid, M. Judd-Ofelt Analysis of Spectroscopic Properties of Eu<sup>3+</sup> Doped KLa(PO<sub>3</sub>)<sub>4</sub>. *J. Lumin.* **2015**, *157*, 21–27. <https://doi.org/10.1016/j.jlumin.2014.08.017>.
- (8) de Sá, G. ; Malta, O. ; de Mello Donegá, C.; Simas, A. ; Longo, R. ; Santa-Cruz, P. ; da Silva, E. . Spectroscopic Properties and Design of Highly Luminescent Lanthanide Coordination Complexes. *Coord. Chem. Rev.* **2000**, *196* (1), 165–195. [https://doi.org/10.1016/S0010-8545\(99\)00054-5](https://doi.org/10.1016/S0010-8545(99)00054-5).